Interaction Notes

Note 241

October 1974

An Improvement on Wire Modeling for Determining the EMP Interaction with Aircraft

C. D. Taylor
K. T. Chen
T. T. Crow
Mississippi State University
Mississippi State, MS 39762

Abstract

An improvement on the wire modeling of an aircraft is accomplished by using intersecting bodies of revolution to represent the aircraft in determining the response to the nuclear electromagnetic pulse (EMP). Extensive aircraft skin current data comparisons for the B-1 aircraft are presented utilizing data from conventional wire models, scale model measurements, and wire mesh models.

This study was performed under subcontract to

The Dikewood Corporation
1009 Bradbury Drive, S.E.
University Research Park
Albuquerque, New Mexico 87106

CONTENTS

Section		Page
I	INTRODUCTION	8
II	ANALYSIS	13
	1. Wire Model of an Aircraft	13
	2. Wire Junctions	20
	3. Intersecting Bodies of Revolution	24
	4. Singularity Expansion Method	27
	5. Ground Alert Mode	27
III.	NUMERICAL RESULTS	28
	1. Comparison with Scale Model Measurements	28
	2. Comparison with Results from Other Models	54
	3. Singularity Expansion Method Result	64
	4. Ground Alert Calculations	65
IV.	CONCLUSION	75
	APPENDIX	76
	REFERENCES	79

ILLUSTRATIONS

Figure		Page
1	B-1 Aircraft with the Wings Forward and the Wings Swept	11
2	B-1 Aircraft in the Ground Alert Mode	12
3	Wire Model of the B-1 used in Computer Code Data Comparison with the University of Michigan Model Measurements. Scale 1:236	14
4	Cylindrical Coordinates used to Express the Electric Field About a Sinusoidal Current Filament	15
5	Two Arbitrarily Oriented Wires with the Necessary Parameters to Specify the Relative Orientation	17
6	Elliptical Body of Revolution with the Appropriate Coordinates	26
7	Comparison of B-1 Model Measurements with Wire Model Results (Top-side Incidence)	30
8	Comparison of B-1 Model Measurements with Results from the Wire Model (Top-side Incidence)	31
9	Comparison of B-1 Model Measurements with Wire Model Results (Top-side Incidence)	32
10	Comparison of B-1 Model Measurements with Wire Model Results (Top-side Incidence)	33
11	Comparison of B-1 Model Measurements with Wire Model Results	34
12	Comparison of B-1 Model Measurements with Results from the Wire Model (Top-side Incidence)	35
13	Comparison of B-1 Model Measurements with Wire Model Results (Top-side Incidence)	36
14	Comparison of B-1 Model Measurements with Results from the wire Model (Top-side Incidence)	37
15	Comparison of B-1 Model Measurements with Wire Model Results (Top-side Incidence)	38

Figure		Page
16	Comparison of B-1 Model Measurements with Wire Model Results (Top-side Incidence)	39
17	Comparison of B-1 Model Measurements with Wire Model Results (Top-side Incidence)	40
18	Comparison of B-1 Model Measurements with Wire Model Results (Top-side Incidence)	41
19	Comparison of B-1 Model Measurements with Results from the Wire Model and the Body of Revolution Model (Top-side Incidence)	42
20	Comparison of B-1 Model Measurements with Results from the Wire Model and the Body of Revolution Model (Top-side Incidence)	43
21	Comparison of B-1 Model Measurements with Results From the Wire Model and the Body of Revolution Model (Top-Side Incidence)	44
22	Comparison of B-1 Model Measurements with Results from the Wire Model and the body of Revolution Model (Top-side Incidence)	45
23	Comparison of B-1 Model Measurements with Results from the Wire Model and the Body of Revolution Model (Top-side Incidence)	46
24	Comparison of B-1 Model Measurements with Results from the Wire Model and the Body of Revolution Model (Top-side Incidence)	47
25	Comparison of B-1 Model Measurements with Results from the Wire Model and the Body of Revolution Model (Top-side Incidence)	48
26	Comparison of B-1 Model Measurements with Results from the wire Model and the body of Revolution Model (Top-side Incidence)	49
27	Comparison of B-1 Model Measurements with Results from the Wire Model & the Body of Revolution Model (Top-side Incidence)	50
28	Comparison of B-1 Model Measurements with Results from the Wire Model and the Body of Revolution Model (Top-side Incidence)	51

Figure		Page
29	Comparison of B-1 Model Measurements with Results from the Wire Model and the Body of Revolution Model (Top-side Incidence)	52
30	Comparison of B-1 Model Measurements with Results from the Wire Model & the Body of Revolution Model (Top-side Incidence)	53
31	Fuselage Current on the B-1 Aircraft at Body Station 5 (Near the Cockpit) Versus Frequency.	55
32	Wire Model Developed at Autonetics for the F-111 Aircraft	56
33	Wire Grid Model Developed at the Boeing Company for the B-1 Aircraft	57
34	Fuselage Current Near Cockpit for the Incident Electric Field Parallel to Fuselage and Topside Incidence	59
35	Comparison of the Results from the Body of Revolution Computer Code with the Results from the Ohio State University Wire Code	60
36	Comparison of the Results from the Body of Revolution Computer Code with the Results from the Ohio State Wire Code	61
37	Comparison of the Results from the Body of Revolution Computer Code with the Results from the Ohio State University Wire Code	62
38	Comparison of the Results from the Body of Revolution Computer Code with the Results from the Ohio State University Wire Code	63
39	Fuselage Current Density for the B-1 in the Ground Alert Mode with Top-side Incidence	67
40	Fuselage Current Density for the B-1 in the Ground Alert Mode with Top-side Incidence	68
41	Fuselage Current Density for the B-1 in the Ground Alert Mode with Top-side Incidence	69
42	Fuselage Current Density for the B-1 in the Ground Alert Mode with Top-side Incidence	70

Figure		Page
43	Wing Current Density for the B-1 in the Ground Alert Mode with Top-Side Incidence	71
44	Wing Current Density for the B-1 in the Ground Alert Mode with Top-Side Incidence	72
45	Wing Current Density for the B-1 in the Ground Alert Mode with Top-side Incidence	73
46	Wing Current Density for the B-1 in the Ground Alert Mode with Top-side Incidence	74
A1	Intersecting Wires with Finite Radii	77

TABLE

Table		Page
1	Resonant and Antiresonant Frequencies for the B-1 Aircraft with Wings Swept	54
2	Natural Frequencies for the B-1 Aircraft	65

SECTION I

INTRODUCTION

The skin currents and charges induced on an aircraft by an electromagnetic pulse, in particular the nuclear EMP, may be determined by using a thin cylinder or wire model of an aircraft and the method of moments (refs. 1, 2, 3 and 4). However, this model has the deficiency that an aircraft fuselage and wings are not sufficiently thin to satisfy all the thin wire theory restrictions. There have been two notable attempts to circumvent this difficulty. First the investigators simply violated thin wire restrictions and calculated skin currents and charges (ref. 1 and 2). This procedure was considered valid because of the good comparison of thin wire theory results with the exact boundary value solution for the current on a prolate spheroid (ref. 3). However it was later observed that numerical instabilities in the current and charge occurred in the vicinity of the wire ends because of violating the restrictions of thin wire approximations (ref. 4). The second attempt to use the thin wire model to represent an aircraft allowed the wires to have as large a radius as possible yet not violate thin wire

---

1. Taylor, C. D. and Crow, T. T., "Induced Electric Currents on Some Configurations of Wires: Part I. Perpendicular Crossed Wires," AFWL Interaction Note 85, November 1971.

2. Crow, T. T., Shumpert, T. H. and Taylor, C. D., "Induced Electric Currents on Some Configurations of Wires: Part II. Non-perpendicular Crossed Wires," AFWL Interaction Note 100, April 1972.

3. Taylor, C. D., "On the Exact Theory of a Prolate Spheroidal Antenna," Radio Science, Vol. 2. (New Series), pp. 351-360, March 1967.

4. Shumpert, T. H., Crow, T. T., and Taylor, C. D., "Induced Electric Currents on Configurations of Thick Wires, Perpendicular Crossed Wires," AFWL Interaction Note 103, May 1972.

considerations (ref. 5). This procedure may not be entirely satisfactory since the peak currents, ringing frequencies, and damping constants all depend upon cylinder radius (ref. 6).

By using the so-called extended boundary, Taylor and Wilton (ref. 7) developed an expeditious formulation valid for thick cylinders as well as bodies of revolution. Applying this formulation Shumpert et al. (ref. 6) have treated intersecting thick wires with flat end faces. Their results did not exhibit the numerical instabilities in the current and charge near the wire ends. However, their formulation did have certain shortcomings. For example, it did not appear to be readily adapted to a complicated configuration of wires with many junctions and their treatment of the wire junctions has not been verified experimentally for wire diameters required in modeling aircraft. Also it would seem more reasonable to model the aircraft with bodies of revolution rather than cylinders with flat end faces.

In this report an electromagnetic model of an aircraft is developed using intersecting bodies of revolution. This is accomplished by using the extended boundary condition, dividing the structure into axial segments and assuming an axial sinusoidal current with unknown coefficients.

---

5. Curtis, W. L., "Current and Charge Distribution on Aircraft," Joint EMP Technical Meeting, Kirtland AFB, September 1973.

6. Taylor, C. D., "A Simple Procedure for Estimating the Current Induced on Cylinder-like Conductors Illuminated by EMP," AFWL Interaction Note 176, July 1973.

7. Taylor, C. D. and Wilton, D. R., "The Extended Boundary Condition Solution of the Dipole Antenna of Revolution," Interaction Note 113, June 1972.

These coefficients are obtained in a procedure analogous to that presented in ref. 8. Various treatments of the wire junctions are considered including the treatment recently developed by King and Wu (ref. 9).

Extensive data are obtained for the induced charge and current on a model of the B-1 aircraft. Results for the induced current density are compared with measured data obtained using a 1:125 scale model of the B-1 (ref. 10). In general the comparison is quite good considering the accuracy of the measurements and the inadequacies of the theoretical model.

Three physical configurations are studied for the B-1. First the inflight mode is considered with the wings forward and with the wings in the full sweep configuration (see fig. 1). Then the ground alert mode is considered with the aircraft in the wings forward configuration (see fig. 2).

Since the time domain response of the induced current and charge is needed in determining the EMP interaction a singularity expansion solution is also obtained. Accordingly natural frequencies, natural modes and coupling coefficients are obtained and presented (ref. 8).

---

8. Crow, T. T., Graves, B. D. and Taylor, C. D., "The Singularity Expansion Method as Applied to Perpendicular Crossed Cylinders in Free Space," AFWL Interaction Note 161, October 1973.

9. King, R. W. P. and Wu, T. T., "Analysis of Crossed Wires in a Plane-wave Field," AFWL Interaction Note 216, July 1974.

10. E. F. Knott, "Surface Field Measurements," AFWL Interaction Application Memo No. 5, September 1974.

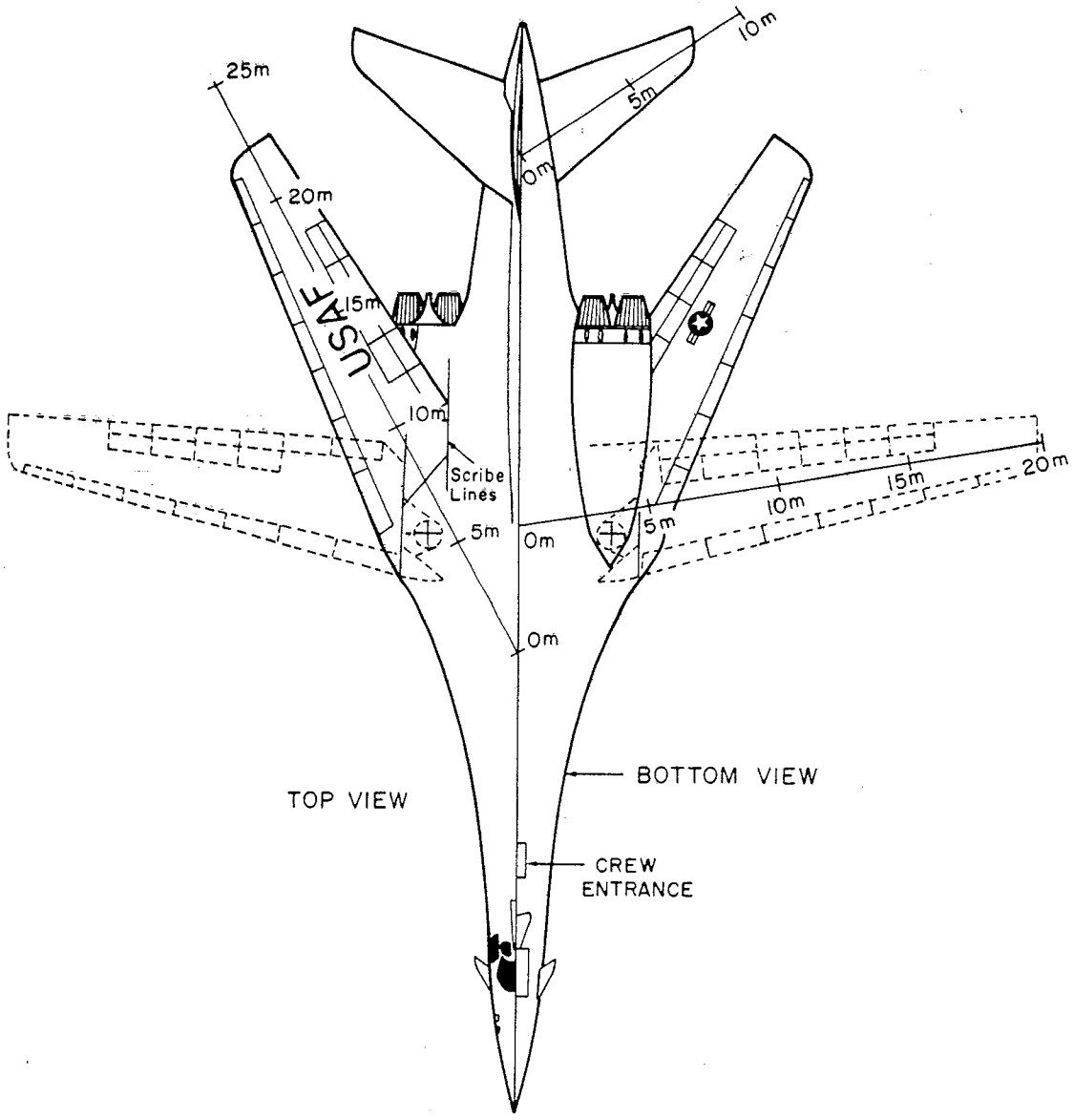

Figure 1: B-1 Aircraft with the Wings Forward and Wings Swept

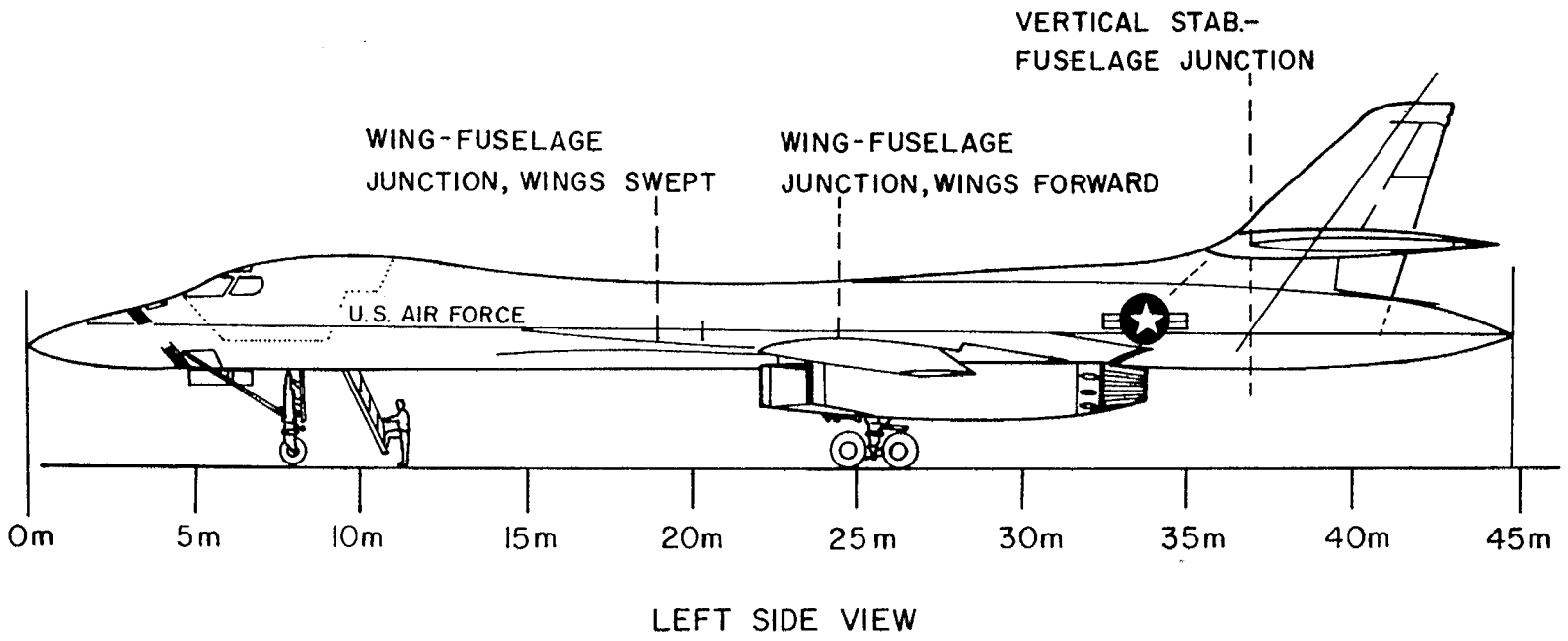

Figure 2: B-1 Aircraft in the Ground Alert Mode

SECTION II

ANALYSIS

1. WIRE MODEL OF AN AIRCRAFT

In developing the wire model of an aircraft the dominant features are represented by wires with appropriate radii and lengths. The wire model for the B-1 aircraft is shown in figure 3. To determine the current induced on the wires by an incident electromagnetic field they are divided into electrically short increments with an assumed sinusoidal current, i.e. for the nth segment of the jth wire with end currents $I_j(s_{j,n})$ and $I_j(s_{j,n+1})$,

$$I_j(s_j) = \frac{I_j(s_{j,n+1})\sin k(s_j - s_{jn}) + I_j(s_{jn})\sin k(s_{j,n+1} - s_j)}{\sin k\,(s_{j,n+1} - s_{jn})} \tag{1}$$

For an infinitesimally thin sinusoidal current filament the accompanying electric field is known exactly (ref. 8). It has two components, an axial component

$$E^{(n)}_{s_j}(\bar{r}) = \frac{1}{4\pi\epsilon j\omega}\left[I_j'(s_{jn})\frac{e^{-jk|\bar{r}-\bar{r}_{jn}|}}{|\bar{r}-\bar{r}_{jn}|} - I_j'(s_{j,n+1})\frac{e^{-jk|\bar{r}-\bar{r}_{j,n+1}|}}{|\bar{r}-\bar{r}_{j,n+1}|}\right] \tag{2}$$

and a radial component (perpendicular to the wire segment as illustrated in figure 4),

$$E^{(n)}_{\rho_j}(\bar{r}) = \frac{1}{4\pi\epsilon j\omega\,\rho_j}\left\{\hat{s}_j' \cdot \left[(\bar{r}-\bar{r}_{j,n+1})I_j'(s_{j,n+1})\frac{e^{-jk|r-r_{j,n+1}|}}{|\bar{r}-\bar{r}_{j,n+1}|} - (\bar{r}-\bar{r}_{jn})I_j'(s_{j,n})\frac{e^{-jk|\bar{r}-\bar{r}_{jn}|}}{|\bar{r}-\bar{r}_{jn}|}\right]\right\} \tag{3}$$

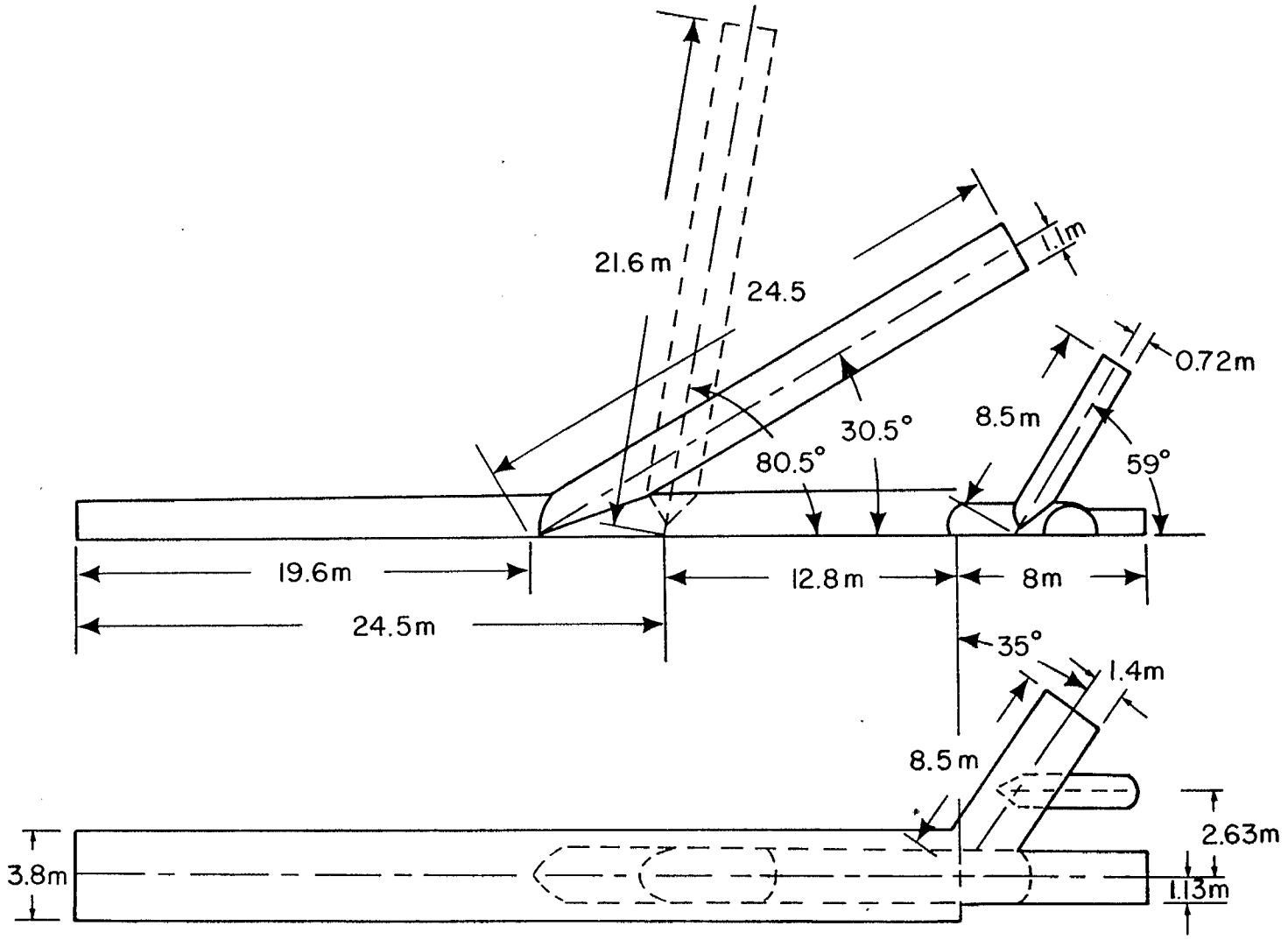

Figure 3: Wire Model of the B-1 used in Computer Code Data Comparison with the University of Michigan Model Measurements. Scale 1:236

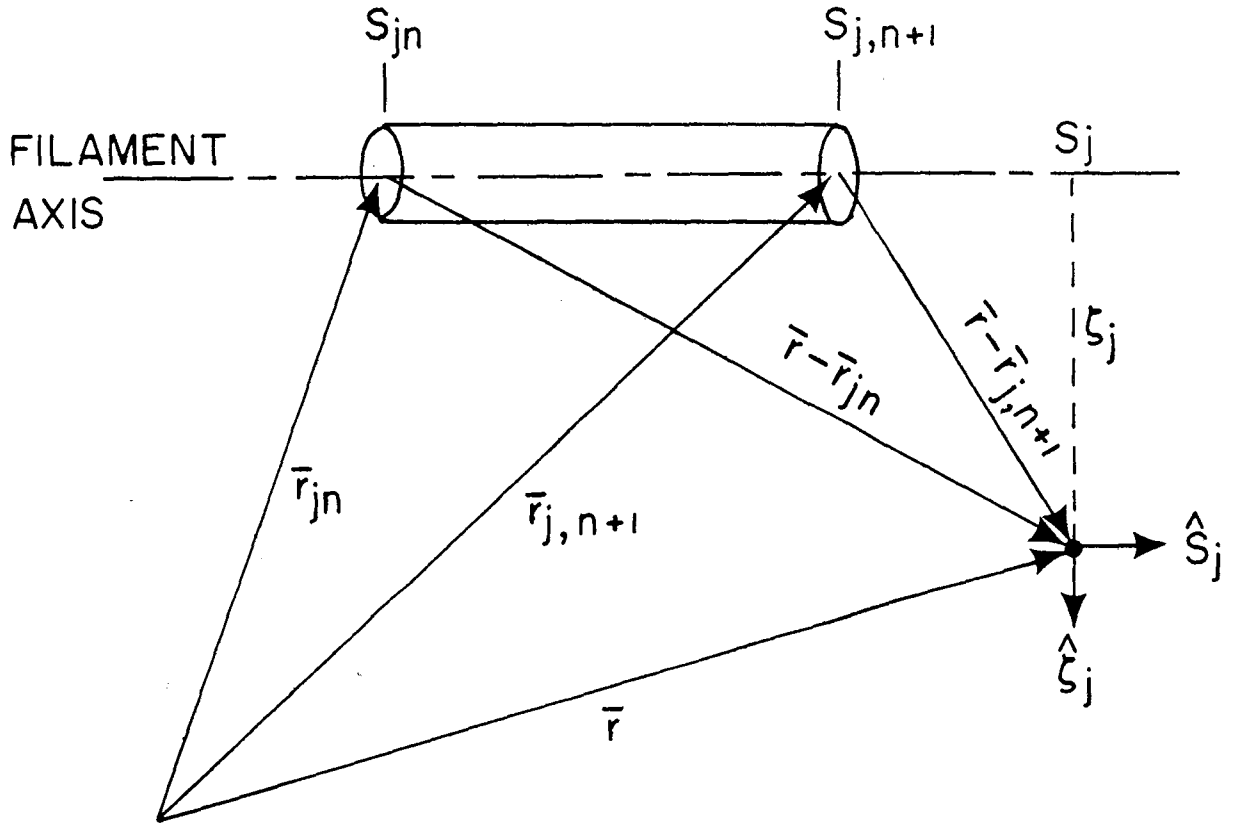

Figure 4: Cylindrical Coordinates Used to Express the Electric Field about a Sinusoidal Current Filament

where

$$I_j'(s_{jn}) = \frac{d}{ds_{jn}} I_j(s_{jn})$$

To illustrate the foregoing technique consider two arbitrarily oriented wires as shown in figure 5. In order to solve for the wire currents, components of the scattered field along each wire axis are needed. For the mth point along the ith wire axis

$$\hat{s}_i \cdot E^{tot}(\bar{r}_{im}) = \hat{s}_i \cdot \bar{E}^{inc}(\bar{r}_{im}) + \sum_{p=1}^{N_i} E_{s_i}^{(p)}(\bar{r}_{im})$$

$$+ \sum_{n=1}^{N_j} \{(\hat{s}_i \cdot \hat{s}_j) E_{s_j}^{(n)}(\bar{r}_{im}) + (\hat{s}_i \cdot \hat{\rho}_j) E_{\rho_j}^{(n)}(\bar{r}_{im})\} \quad (4)$$

and an analogous expression may be obtained for points along the jth wire. Here N_i and N_j are the numbers of increments along the ith and jth wire respectively, and $E_{s_i}^{(p)}(\bar{r}_{im})$ is the contribution to the axial component along the ith wire from the pth increment of the ith wire and is called the self-field contribution. And the electric field components $E_{s_j}^{(n)}(\bar{r}_{im})$ and $E_{\rho_j}^{(n)}(\bar{r}_{im})$ account for the coupling of the currents between the ith and jth wires. If the wires are solid then the end cap current and charge contributions should also be included in eqn. (4) as discussed in ref. 7.

The terms appearing in (4) are

$$E_{s_i}^{(p)}(\bar{r}_{im}) = \frac{1}{4\pi\varepsilon j\omega} [I_i'(s_{ip})\, K_o(s_{im}, s_{ip}) - I_i'(s_{i,p+1})\, K_o(s_{im}, s_{i,p+1})] \quad (5)$$

$$E_{s_j}^{(n)}(\bar{r}_{im}) = \frac{1}{4\pi\varepsilon j\omega} [I_j'(s_{jn})\, K_o(s_{im}, s_{jn}) - I_j'(s_{j,n+1})\, K_o(s_{im}, s_{j,n+1})] \quad (6)$$

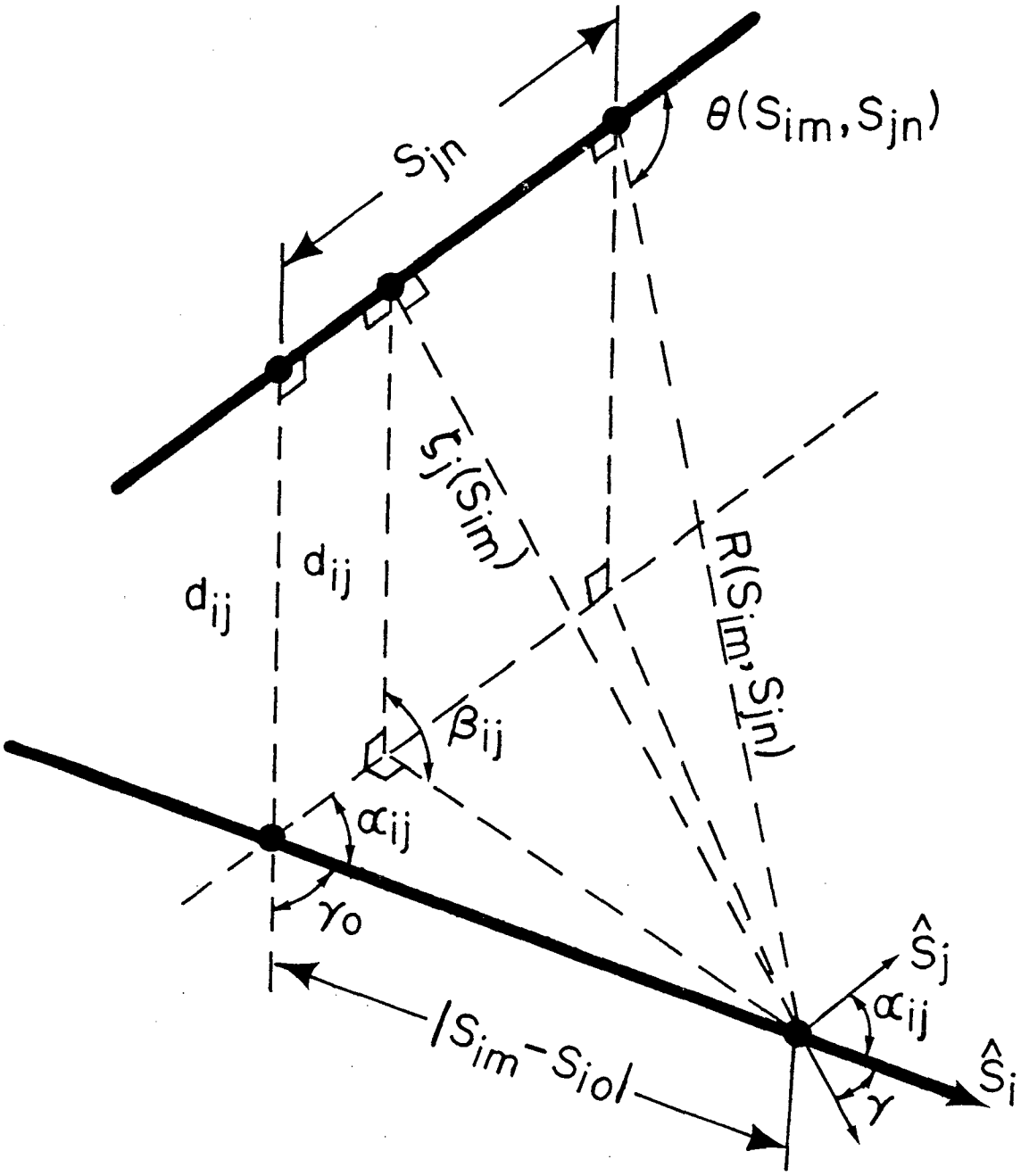

Figure 5: Two Arbitrarily Oriented Wires with the Necessary Parameters to Specify the Relative Orientation

$$E^{(n)}_{\rho_j}(\bar{r}_{im}) = \frac{1}{4\pi\epsilon j\omega}\frac{1}{\sqrt{\rho_j^2(s_{im})+ a_j^2}}\cos[\theta(s_{im},s_{j,n+1})]e^{-jkR(s_{im},s_{j,n+1})}$$

$$-\cos[\theta(s_{im},s_{jn})]e^{-jkR(s_{im},s_{jn})}\} \qquad (7)$$

where

$$K_o(s_{im},s_{jn}) = \exp\,[-jkR(s_{im},s_{jn})]/R(s_{im},s_{jn}) \qquad (8)$$

$$\rho_j(s_{im}) = [d_{ij}^2 + (s_{im} - s_{io})^2 \sin^2\alpha_{ij}$$

$$- 2(s_{im} - s_{io})d_{ij}\cos\beta_{ij}\sin\alpha_{ij}]^{\frac{1}{2}} \qquad (9)$$

$$R(s_{im},s_{jn}) = \{\rho_j^2(s_{im}) + [(s_{jn} - s_{jo}) - (s_{im} - s_{io})\cos\alpha_{ij}]^2$$

$$+ a_j^2\}^{\frac{1}{2}} \qquad (10)$$

$$\hat{s}_i \cdot \hat{s}_j = \cos\alpha_{ij} \qquad (11)$$

$$\hat{s}_i \cdot \hat{\rho}_j = \frac{(s_{im} - s_{io})\sin^2\alpha_{ij} - d_{ij}\cos\beta_{ij}\sin\alpha_{ij}}{\rho_j(s_{im})} \qquad (12)$$

$$\cos\theta(s_{im},s_{jn}) = \frac{-(s_{jn} - s_{jo}) + (s_{im} - s_{io})\cos\alpha_{ij}}{R(s_{im},s_{jn})} \qquad (13)$$

with α_{ij}, β_{ij}, d_{ij}, s_{io} and s_{jo}, defined as shown in figure 5, depending on the relative orientation of the wires. With the foregoing it is straight forward, albeit tedious, to set up the system of algebraic equations for the currents, $I_j(s_{jn})$ for $j = 1, N$ and $n = 1, N_j + 1$, where N is the total number of wires and N_j the number of increments used on the jth wire.

The foregoing expressions are used to determine the total field about the wire configuration. To obtain a system of linear algebraic equations for the end currents of the wire increments, $I_j(s_{jn})$, the total electric field (incident + scattered) component tangent to the wire axes is set equal to zero at a discrete set of points along the axes of all wires. Since eqns. (2) and (3) are valid only for current filaments some modification is required to treat current on wires with nonzero radius. If the wires are electrically thin, the induced current density on the wire is uniformly distributed about the cross section. Then the surface of the wire segment may be divided into identical filamentary strips. In the appendix an expression for the average radial distance is obtained. Using this average radial distance in eqns. (2) and (3), i.e. letting

$$|\vec{r} - \bar{r}_{jn}| \rightarrow \sqrt{|\bar{r} - r_{jn}|^2 + a_j^2}$$

$$|\bar{r} - \bar{r}_{j,n+1}| \rightarrow \sqrt{|r - r_{j,n+1}|^2 + a_j^2}$$

$$\rho_j \rightarrow \sqrt{\rho_j^2 + a_j^2}$$

yields corresponding expressions valid for wires with nonzero radius. For field points along the wire axis the obtained expressions are exact. It is these expressions that are used to determine the total electric field component set equal to zero at a discrete set of points along the axes of all the wires of the configuration. For best results these points are selected to be the end points of the wire increments.

In addition to the foregoing some condition is imposed on the wire currents and/or charges at all junctions. This topic is discussed in the next section.

2. WIRE JUNCTIONS

A number of techniques for treating wire junctions have been suggested. It was Schelkunoff who first suggested that the Kirchhoff current law and the continuity of scalar potential be imposed at the wire junction (ref. 11). The scalar potential condition is necessary only when the Hallèn-type integral equations are used (ref. 12). These conditions are strictly valid only for very thin wires and they avoid the consideration of the somewhat complicated flow of charge within the junction region.

Later Chao and Strait developed another junction treatment (ref. 13). They consider the wire junction to be formed by overlapping wire segments (see figure 3). Since they use the Pocklington-type integral formulation there was no need to require explicitly the continuity of scalar potential, and the effect of the overlapping wire segments is to insure that the Kirchhoff current law is satisfied. Thus as would be expected their results agree quite well with those obtained from the

---

11. Schelkunoff, S. A. and Friis, H. T., Antennas: Theory and Practice. John Wiley, New York, 1952.

12. Mei, K. K., "On the Integral Equations of Thin Wire Antennas," IEEE Trans. Ant. Prop., AP-13, pp. 374-378, May 1965.

13. Chao, H. H. and Strait, B. J., "Computer Programs for Radiation and Scattering by Arbitrary Configurations of Bent Wires," AFWL Interaction Note 191, September 1970.

Hallén-type integral equation formulations with the Kirchhoff current law and continuity of scalar potential imposed (ref. 14). It should be mentioned that Richmond's formulation for wire configurations employing the use of the reaction concept also uses the Chao and Strait junction treatment (ref. 15).

Another treatment of the wire junction is suggested by Sayre (ref. 16). He suggests that the continuity equation be applied in its general form in the vicinity of the junction. An imaginary spherical surface is considered to enclose the junction region with the center of the sphere coincident with the junction of the wire axes. Accordingly he obtains for a junction of N wires

$$\sum_{j=1}^{N} I_j = -j\omega N\langle q\rangle$$

where I_j is the current on the jth wire at the aforementioned spherical surface and $\langle q\rangle$ is the average charge on each of the wire segments inside the imaginary spherical surface. Allowing the radius of the imaginary surface to become vanishingly small yields the Kirchhoff current law. Sayre claimed that his technique is more convenient to use than the treatment used by Chao and Strait. Also his numerical results compare quite well with the data obtained by Chao and Strait.

---

14. Butler, C. M., "Currents Induced on a Pair of Skew Crossed Wires," IEEE Trans. Ant. Prop., AP-20, pp. 731-736, November 1972.

15. Richmond, J. H., Schwab, L. M., and Wickliff, R. G., "Tumble-Average Radar Backscatter of Some Thin-Wire Chaff Elements," IEEE Trans. Ant. Prop., AP-22, pp. 124-126, January 1974.

16. Sayre, E. P., "Junction Discontinuities in Wire Antenna and Scattering Problems," IEEE Trans. Ant. Prop., AP-21, pp. 216-217, March 1973.

A junction treatment very similar to that proposed by Sayre is suggested by Curtis (ref. 5). He also uses the continuity equation in the integral form and an imaginary surface. In particular he uses

$$\sum_{j=1}^{N} I_j = -j\omega Q$$

where I_j is the current on the jth wire at the imaginary surface enclosing the junction and Q is the total charge contained within the surface. Further he considers the total charge to be distributed uniformly over the junction surface and imposes continuity of charge on each wire at the imaginary surface. Computations using Curtis' junction technique have been made and compared with the Chao and Strait results (ref. 17). Again quite good agreement is obtained.

Recently Crow et al. have developed a Pocklington-type integral equation formulation that uses only the Kirchhoff current law at the wire junction (ref. 8). That is, for a junction of N wires the currents at the center of the junction satisfies

$$\sum_{j=1}^{N} I_j = 0$$

Numerical data have been obtained that are in good agreement with the results of the foregoing junction treatments.

Very recently Mittra and Ko showed that the numerical solution to the Pocklington-type integro differential equation for the currents near

---

17. Miller, E. K., Bevensee, R. M., Poggio, A.J., Adams, R., Deadrick, F.J., and Landt, J. A., "An Evaluation of Computer Programs Using Integral Equations for the Electromagnetic Analysis of Thin Wire Structures," AFWL Interaction Notes, Note 177, March 1974.

a wire junction can be obtained without imposing any junction condition (ref. 18). Their solution technique did involve a judicial choice of match points and the use of finite differences. However, their results are in excellent agreement with the results of the aforementioned formulations.

An experimental investigation of wire currents and charges near the junction of intersecting thin cylinders has been performed more recently by King and Burton (ref. 19). Perhaps the most significant observations made concerned the behavior of the current and charge near the junction. Specifically they found that the Kirchhoff current law is satisfied and that the charge density is continuous and smoothly varying through the junction region.

Reconsidering junction conditions in light of the King and Burton measurements, King and Wu argue that requiring continuity of scalar potential is not a valid junction condition to impose since it does not assure continuity of charge through the junction unless the wires are very thin (ref. 9). Moreover they argue that for the Hallén-type integral equation formulation the Kirchhoff current law and continuity of charge form a set of necessary and sufficient conditions to be imposed at wire junctions. Although their arguments are not rigorous they nevertheless are convincing for the junction conditions to be used with the Hallén-type integral equation formulation.

---

18. Mittra, R. and Ko, W. L., "A Finite Difference Approach to the Wire Junction Problem," to be submitted for publication.

19. King, R. W. P. and Burton, R., private communication.

From the foregoing discussion it must be concluded that if the Hallén-type integral formulation is used to determine the currents induced on a configuration of intersecting wires, the King and Wu junction conditions should be used. However,if the Pocklington-type integro-differential equation formulation is used no junction conditions are necessary. But valid junction conditions may be used for convenience. As will be reported subsequently various junctions are used to determine the dependence of the current solution on the junction treatment used.

3. INTERSECTING BODIES OF REVOLUTION

Using a solid wire model of an aircraft presents two difficulties. First, the dominant features of an aircraft are not cylindrical and second, the wire end faces will be sufficiently large that the existing current and charge on the ends have an appreciable effect on the induced current and charge over the entire structure. However, if the dominant features of an aircraft are modeled by bodies of revolution the extended boundary condition formulation of Taylor and Wilton (ref. 7) can be used. Moreover the body of revolution is a closer physical approximation.

Considering the body of revolution in the model does increase the complexity of the formulation and the resulting computer code. The self electric field along the axis of a body of revolution is (ref. 7)

$$4\pi\varepsilon j\omega\, E^{(n)}_{s_i}(\bar{r}_{im}) = \int_{s_{in}}^{s_{i,n+1}} ds_i\, I_i(s_i)\left[k^2 - \frac{\partial}{\partial s_i}\frac{\partial}{\partial s_{im}} K(s_{im},s_i)\right] + I_i(s_i)\frac{\partial}{\partial s_{im}} K(s_{im},s_i)\Big|_{s_{in}}^{s_{i,n+1}} \qquad (14)$$

where

$$K(s_{im},s_i) = \exp[-jk\sqrt{(s_{im}-s_i)^2 + a_i^2(s_i)}]/\sqrt{(s_{im}-s_i)^2 + a_i^2(s_i)} \qquad (15)$$

A comparison of the body-of-revolution model with the wire model is given in fig. 6.

Using eqn. (14) allows the ready determination of the self-electric field component which may be combined with the wire approximations for the coupling electric field components of eqns(4), (5), (6) and (7). Inasmuch as the self-electric field is generally an order of magnitude more significant than the coupling electric field for electrically thin structures, $\lambda >> a$, this approach should yield highly accurate results and yet allow for very complex current paths. Of course the radial variation with axial length may be chosen to conform with the actual aircraft. However, for the study reported here a convenient elliptical variation is considered (see fig. 6). Then

$$a_i(s_i) = a_i(c_i)\left[\frac{2(L_i-c_i)(L_i-s_i) - (L_i-s_i)^2}{(L_i-c_i)^2}\right]^{1/2} \qquad (16)$$

where $s_i = L_i$ locates the free end of the body and $s_i = c_i$ locates the junction with other bodies. There are two sections of the B-1 aircraft, namely the section of the fuselage between the wings and vertical stabilizer and the section of the vertical stabilizer between the fuselage and horizontal stabilizer, that are more conveniently modeled by cylinders in which case eqn. (16) is not applicable. Otherwise eqn. (16) is used to represent the B-1 aircraft features. In the coupling electric field component expressions the radii

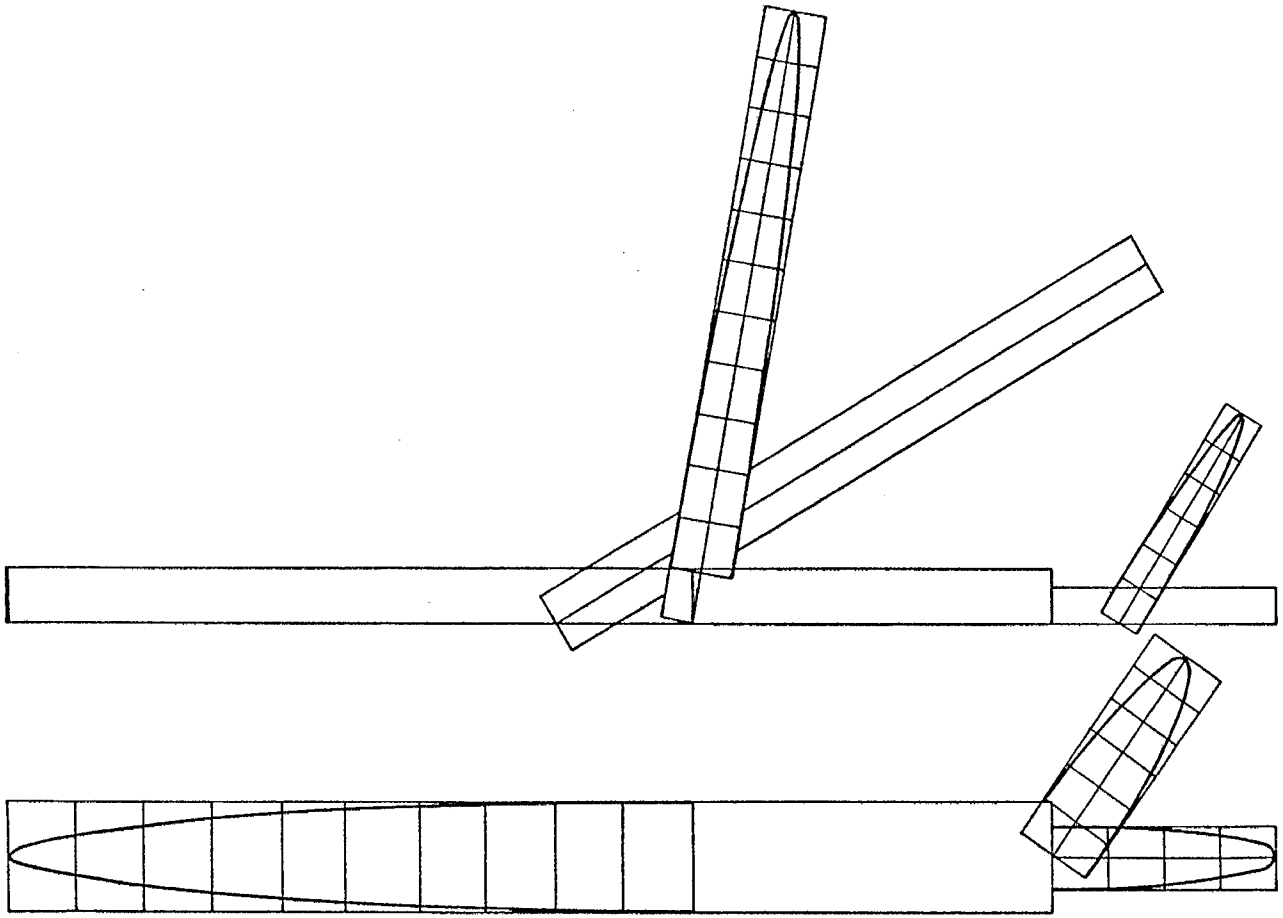

Figure 6. Comparison of B-1 Wire Model and Elliptical Body-of-Revolution Model Used in Present Calculations

$$a_i = a_i(c_i)$$

are used.

4. SINGULARITY EXPANSION METHOD

The nuclear EMP being an electromagnetic pulse requires a time domain formulation be developed. As reported in ref. 8, the singularity expansion method is quite convenient in determining the time domain behavior of the currents and charges induced by an incident pulse. The authors defer to ref. 8 for the details of this technique and only the results will be reported here.

5. GROUND ALERT MODE

In the ground alert mode the aircraft is located only a few meters above the ground (see fig. 2) and the wings of the aircraft are in the forward configuration. If the aircraft is illuminated by a line source parallel to the ground then the induced current on the aircraft becomes even more difficult to obtain. First the ground reflects the signal from the source and the signal scattered from the aircraft is reflected from the ground back onto the aircraft. However, both processes may be accounted for by use of image theory.

SECTION III

NUMERICAL RESULTS

In order to apply the formulation developed in the foregoing, dimensions appropriate to the B-1 aircraft are considered (see fig. 3). Extensive calculations are made for comparisons with measured data and other theoretical predictions.

1. COMPARISON WITH SCALE MODEL MEASUREMENTS

The purposes for comparing the theoretical results with scale model measurements are two fold. First there is the obvious purpose; the comparison is used to verify the theoretical model. Second the comparison is used to determine the best junction treatment.

For the scale model measurements of ref. 10 the illumination of the aircraft is propagating perpendicular to the aircraft fuselage and wings. The surface current densities are measured on the topside of the fuselage and wings, the incident side of the aircraft. Since the model used in the test is plastic with a complete and uniform metallic coating, agreement of the theoretical results with model measurements should be better than the agreement with the actual aircraft skin current measurements.

Model measurements are presented for four frequencies and two wing orientations--wings forward and wings swept. First the theoretical data are compared with model measurements to determine the appropriate junction treatment. Here only the wire model shown in figure 3 is used in obtaining the theoretical data for three junction treatments--enforcing continuity of surface charge density, enforcing the Kirchhoff

current law, and enforcing both the continuity of charge density and the Kirchhoff current law. In order to maintain a sufficient number of equations to obtain the unknown axial current for the three junction conditions, match points at the center of the junction were used or deleted as required. As seen from figures 7 through 18, the continuity of charge plus the Kirchhoff current law usually yields the best comparison with the experimental data. However, the other junction conditions did yield good results as had been observed previously (ref. 8).

Having determined the best junction treatment the results from the wire model formulation are compared with the results from the body of revolution formulation. These data are shown in figures 19 through 30. In general the body of revolution data are appreciably in better agreement with the experimental data. For the data that are presented the body of revolution results are typically within 10 dB of the measured data except in the regions of current nulls where the theoretical data generally exhibit deeper nulls and in the region of the tail structure where existing sharp edges concentrate current not accounted for in the theory. It must be concluded that the body of revolution does provide a reasonable electromagnetic model of an aircraft. It is also noted that the wire model yields very good results. Since the computation time required for the body of revolution computer code exceeds that required for the wire model code, the wire model code may be preferred in many cases.

In selecting the frequencies at which the skin current measurements are presented, the induced current was observed over a range of

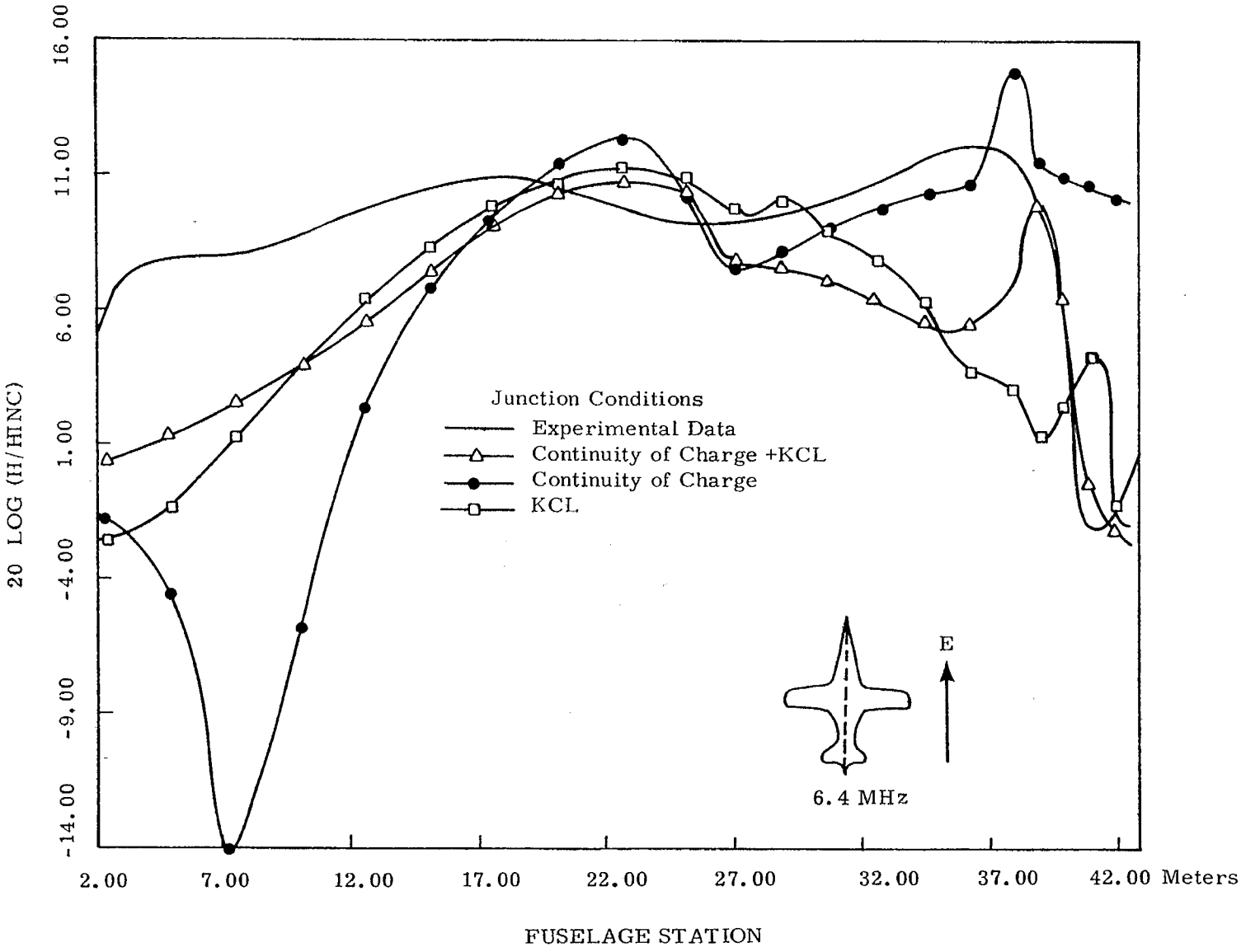

Figure 7: Comparison of B-1 Model Measurements with Wire Model Results (Top-side Incidence)

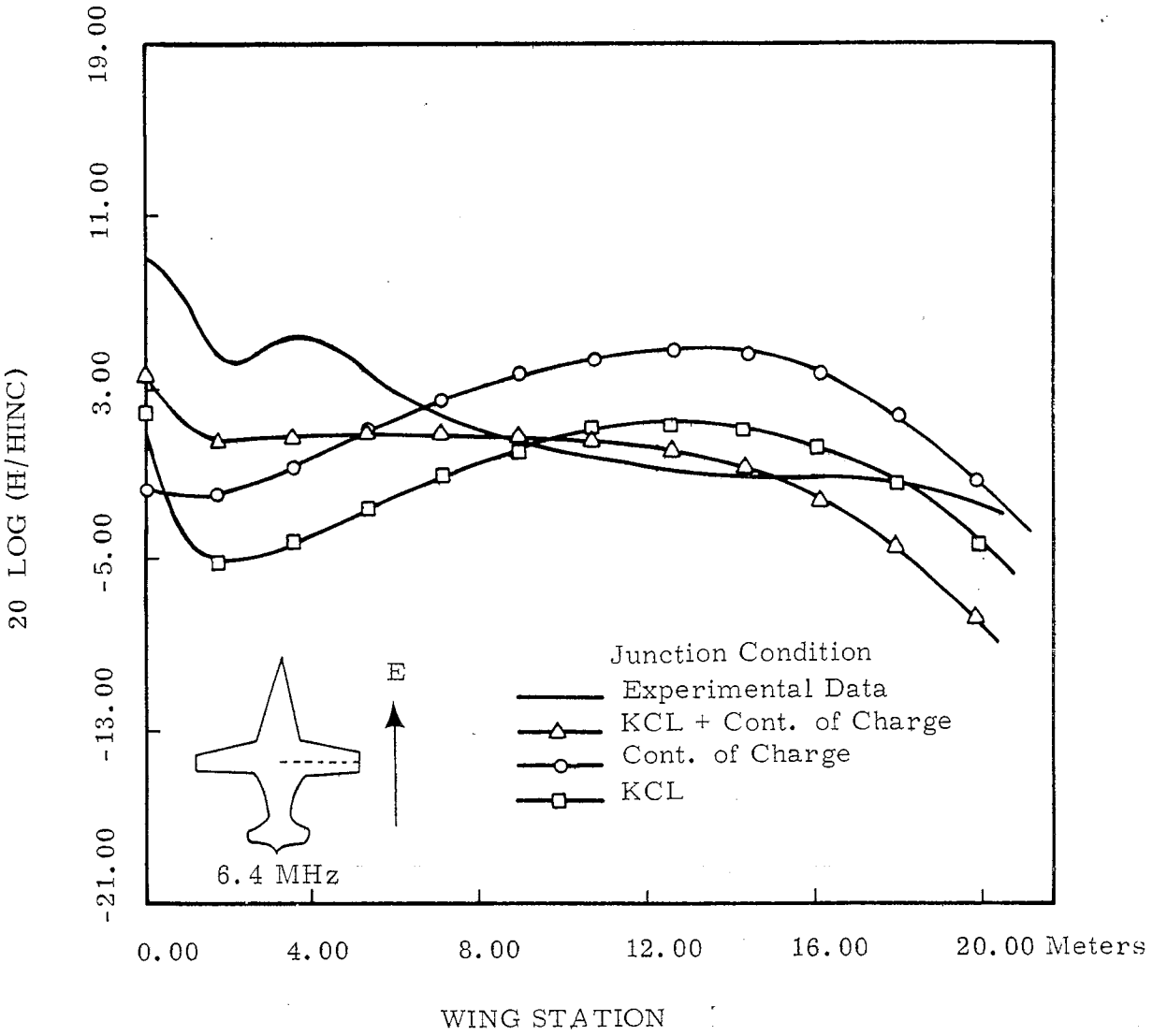

Figure 8: Comparison of B-1 Model Measurements with Results from the Wire Model (Top-side Incidence)

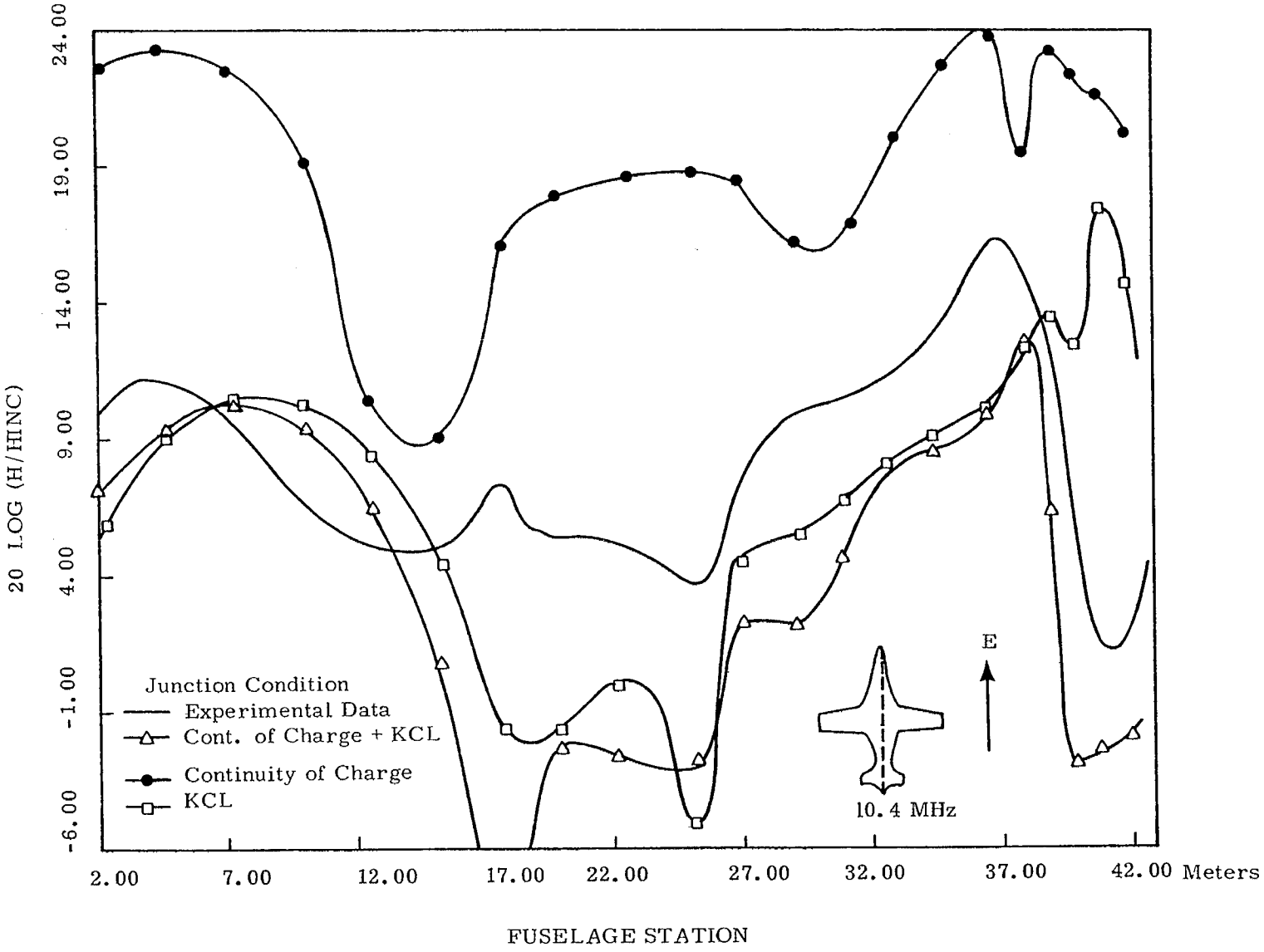

Figure 9: Comparison of B-1 Model Measurements with Wire Model Results (Top-side Incidence)

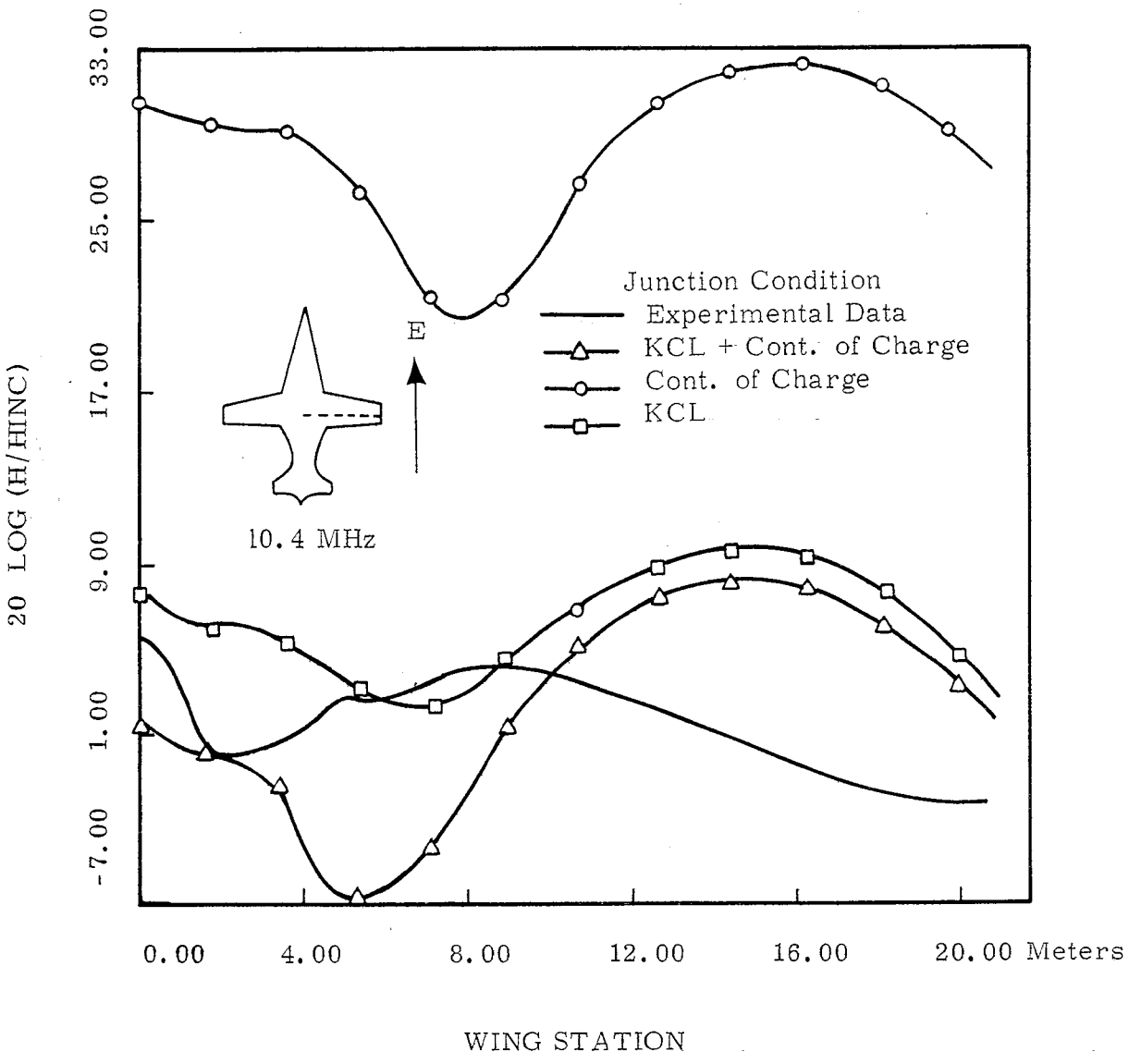

Figure 10: Comparison of B-1 Model Measurements with Wire Model Results (Top-side Incidence)

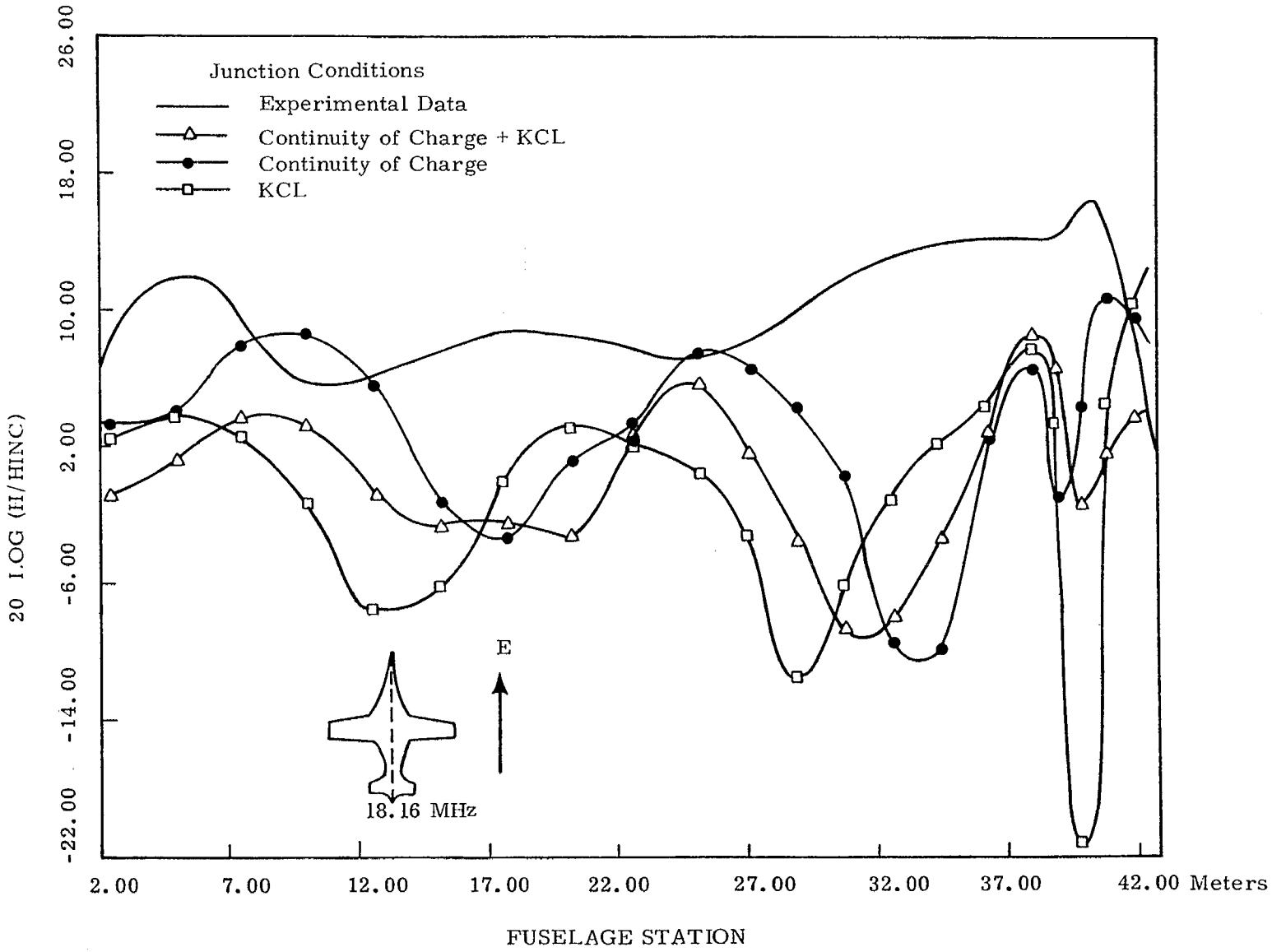

Figure 11: Comparison of B-1 Model Measurements with Wire Model Results (Top-side Incidence)

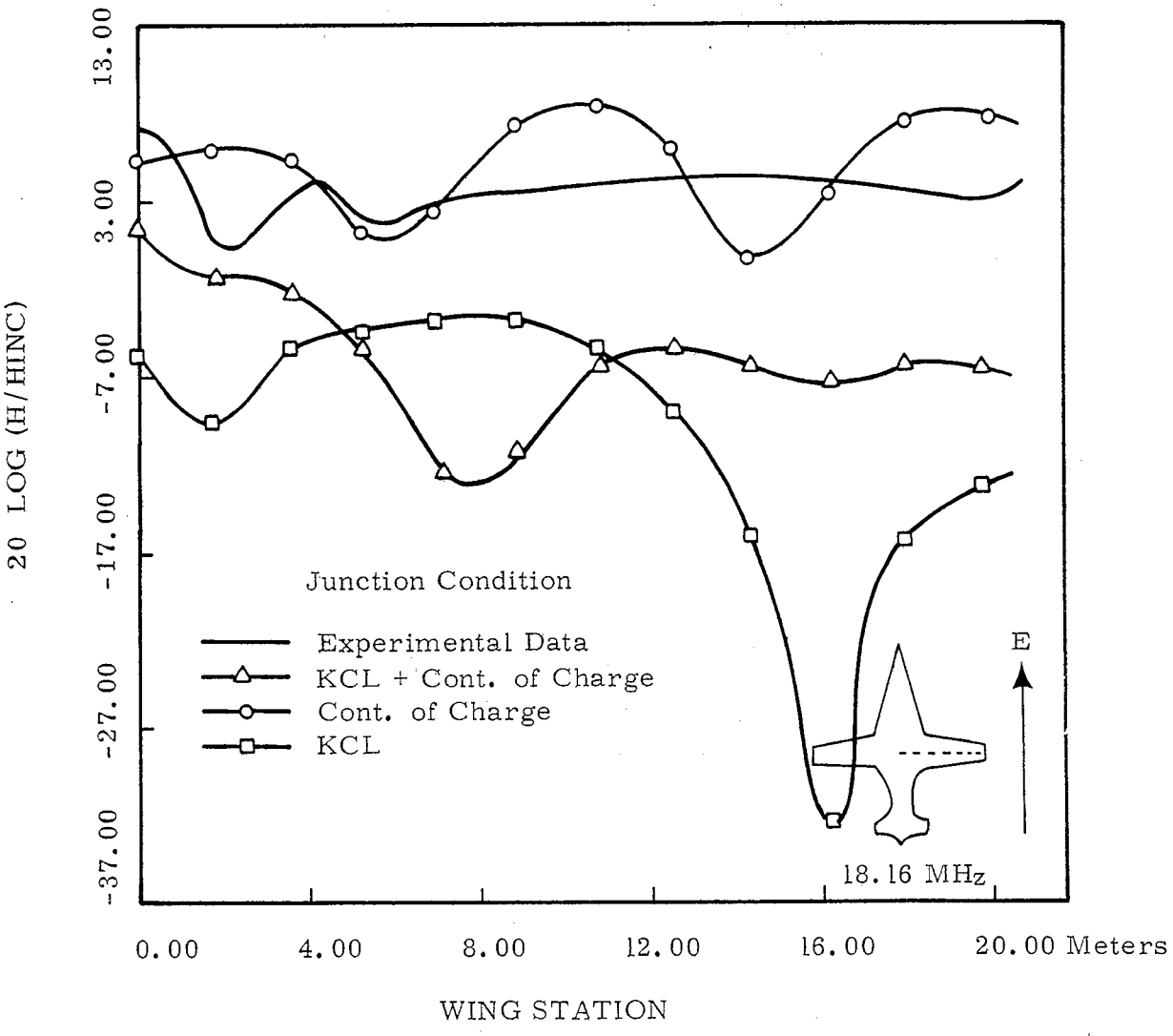

Figure 12: Comparison of B-1 Model Measurements with Results from the Wire Model (Top-side Incidence)

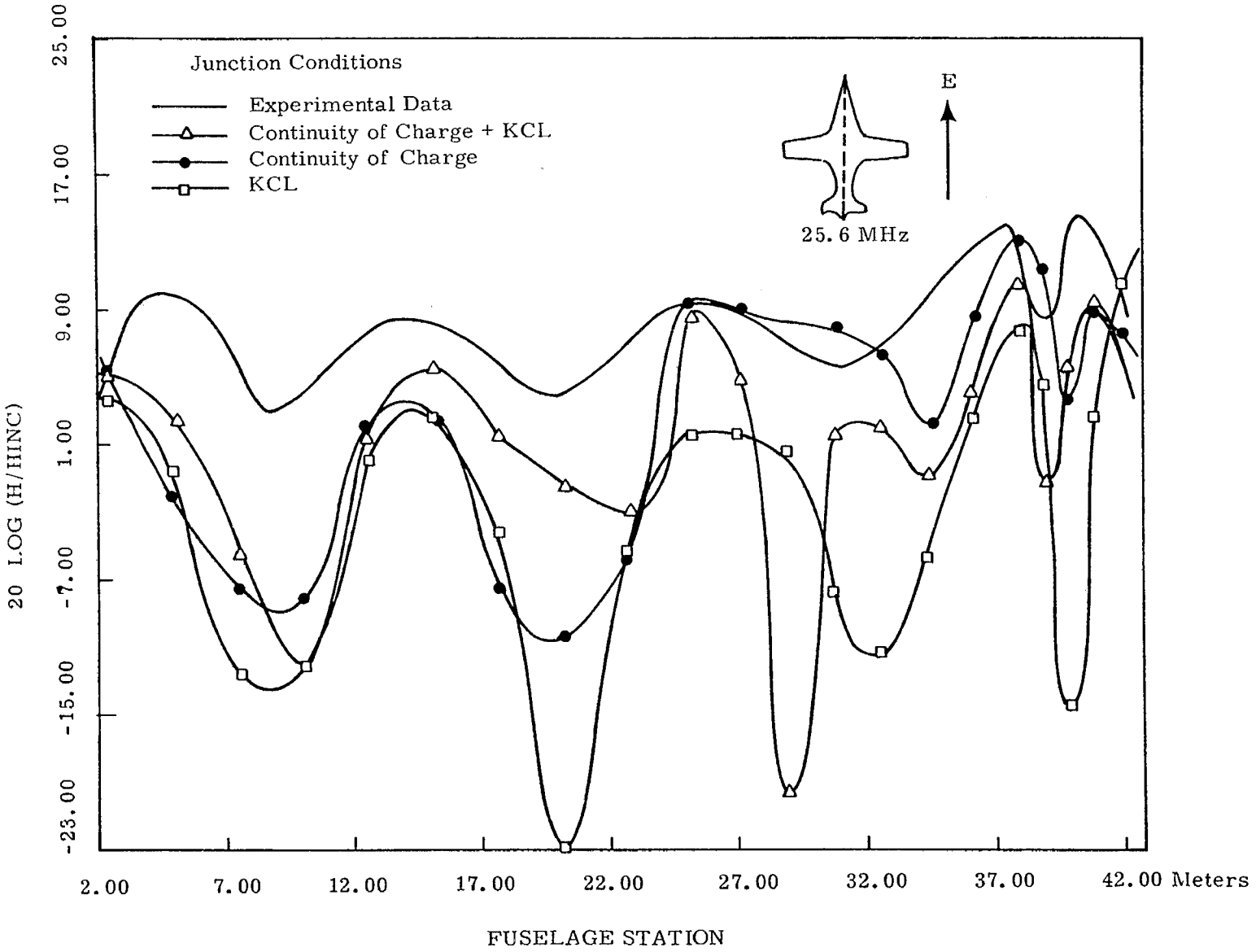

Figure 13: Comparison of B-1 Model Measurements with Wire Model Results (Top-side Incidence)

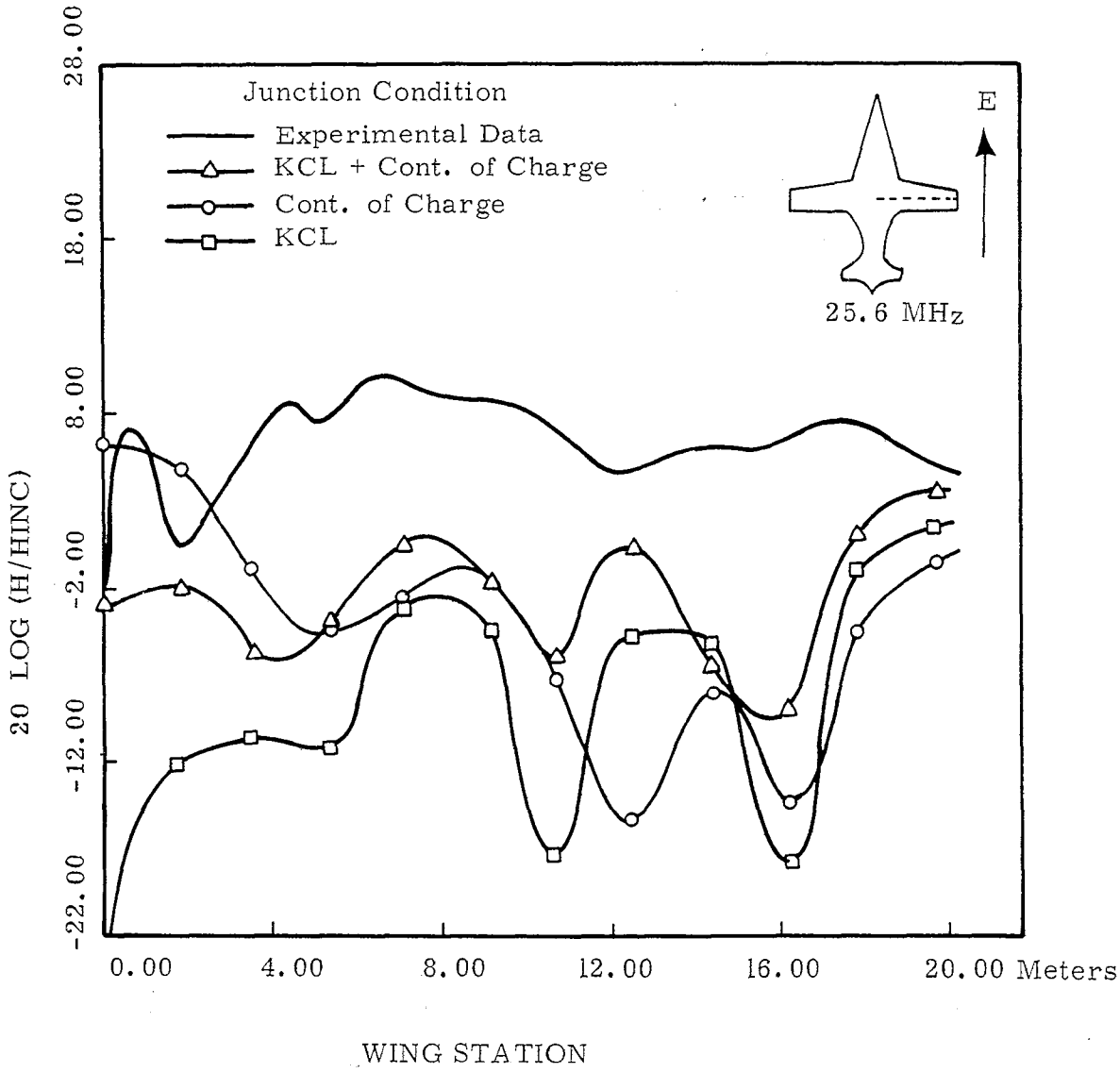

Figure 14: Comparison of B-1 Model Measurements with Results from the Wire Model (Top-side Incidence)

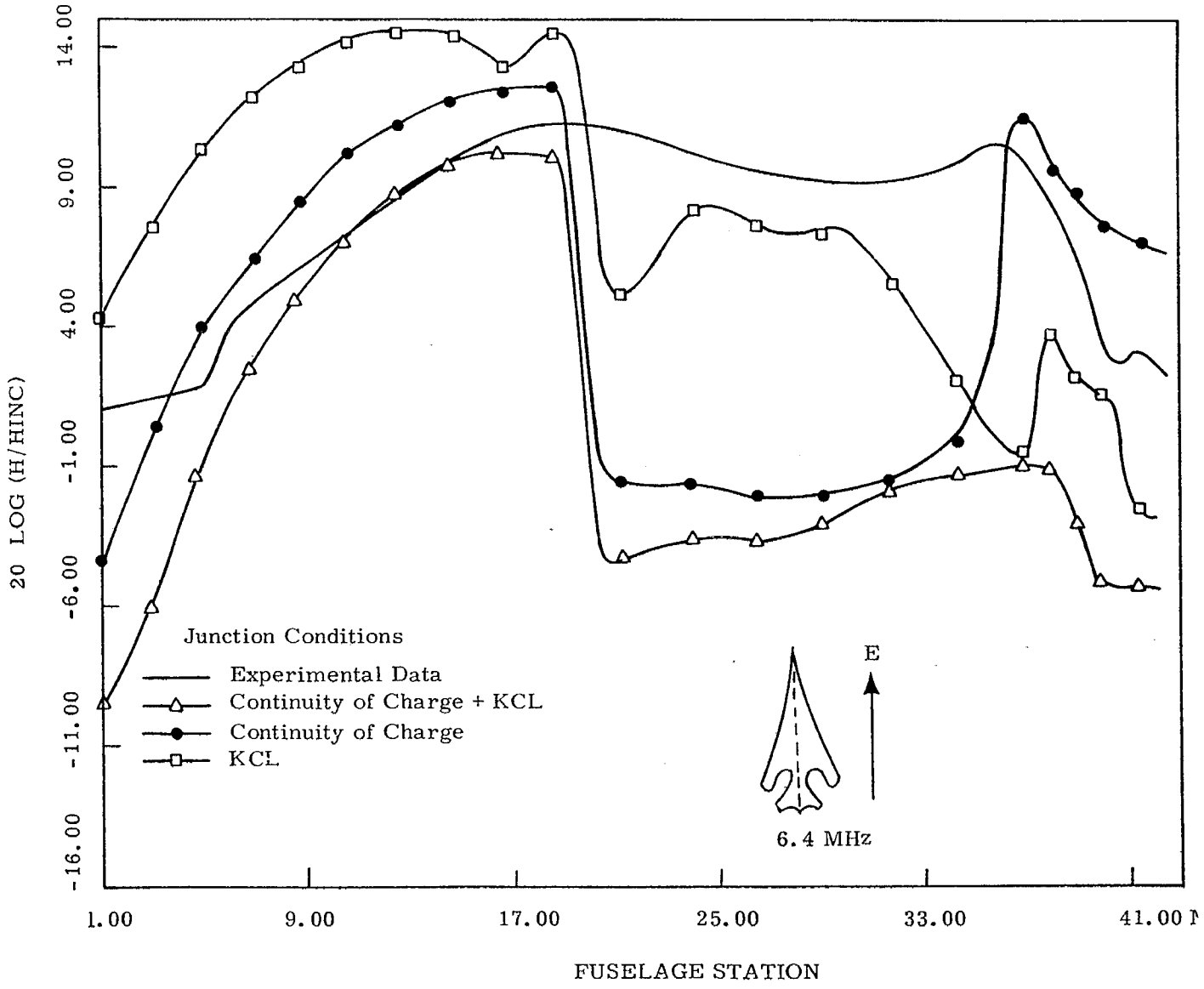

Figure 15: Comparison of B-1 Model Measurements with Wire Model Results (Top-side Incidence)

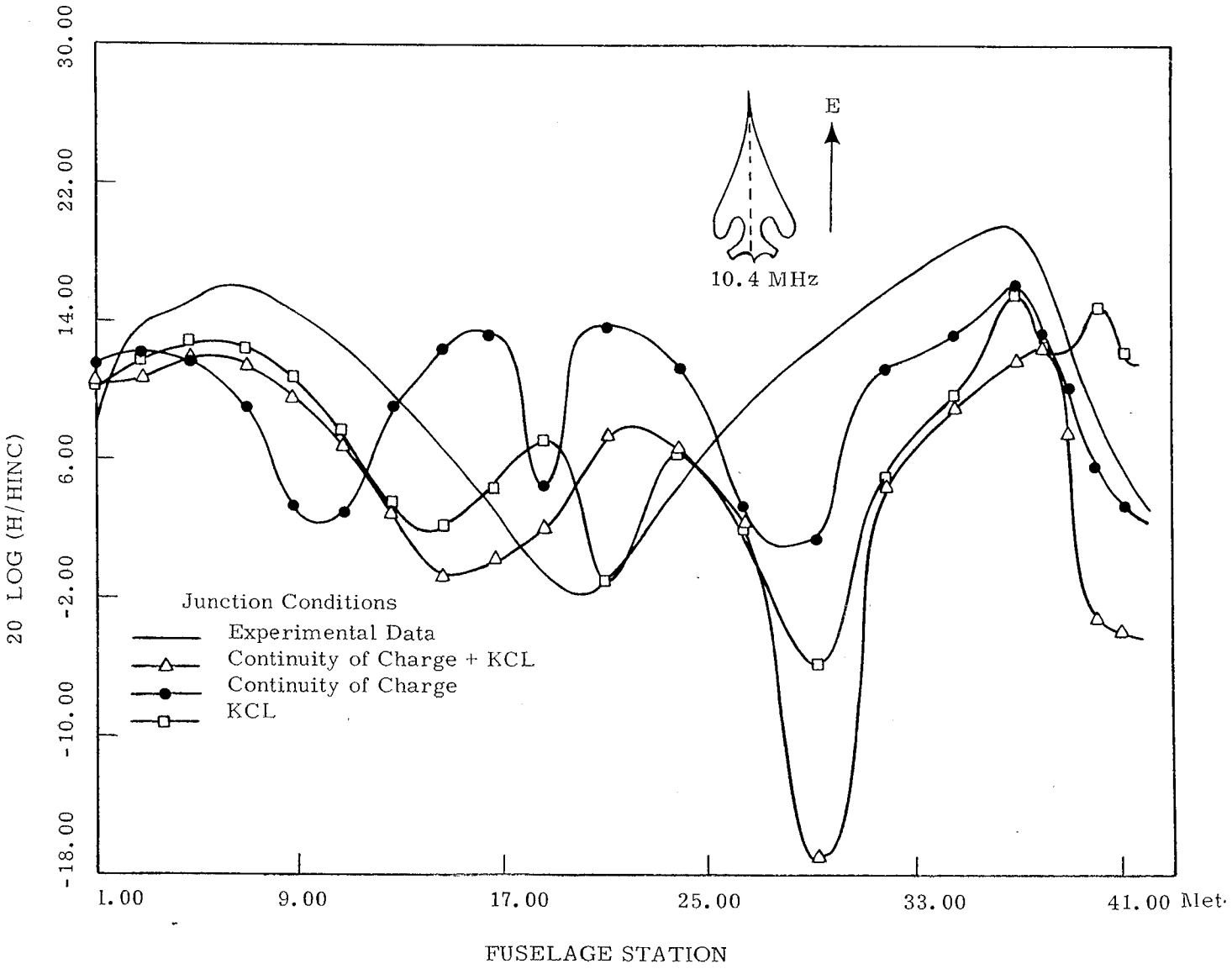

Figure 16: Comparison of B-1 Model Measurements with Wire Model Results (Top-side Incidence)

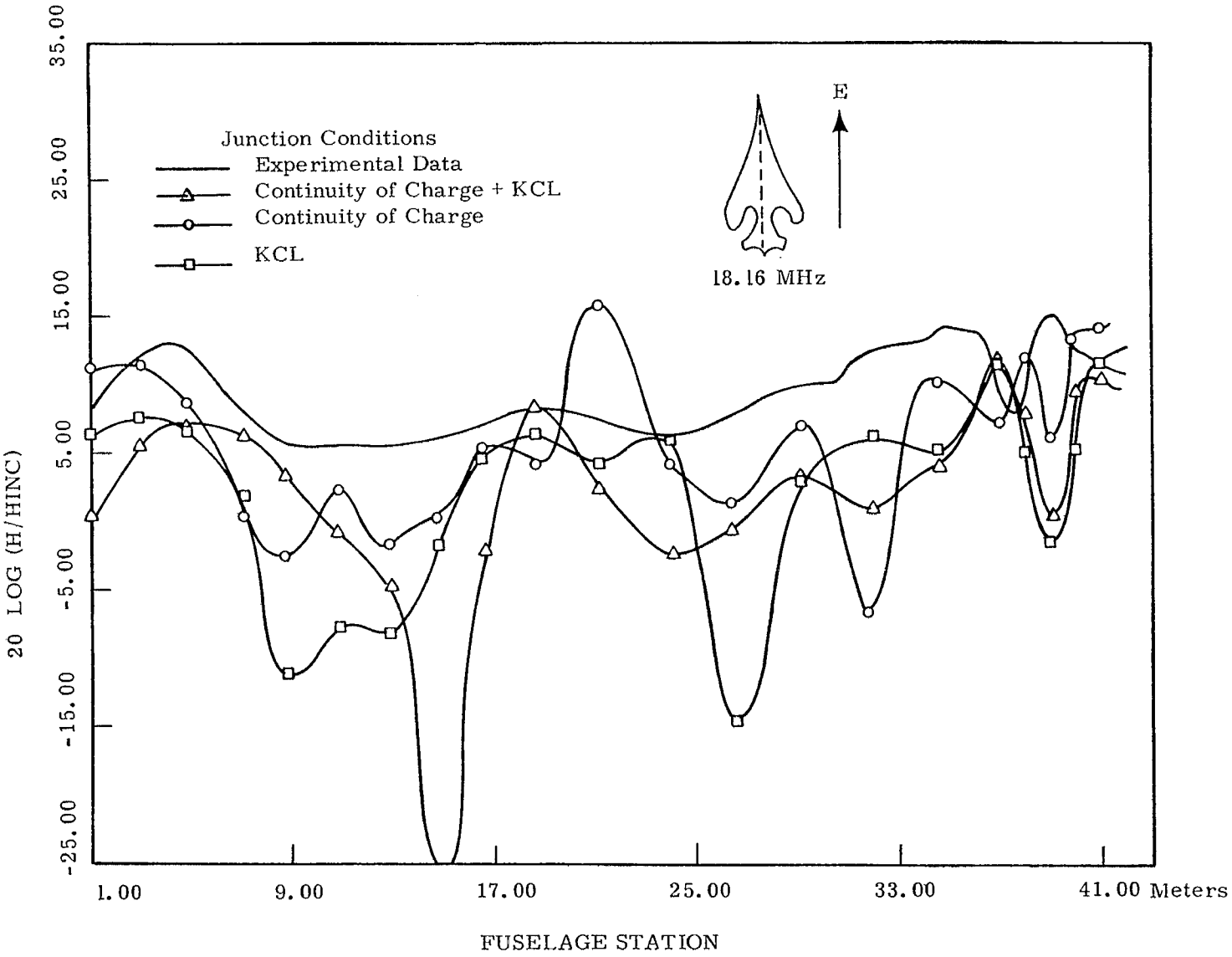

Figure 17: Comparison of B-1 Model Measurements with Wire Model Results (Top-side Incidence)

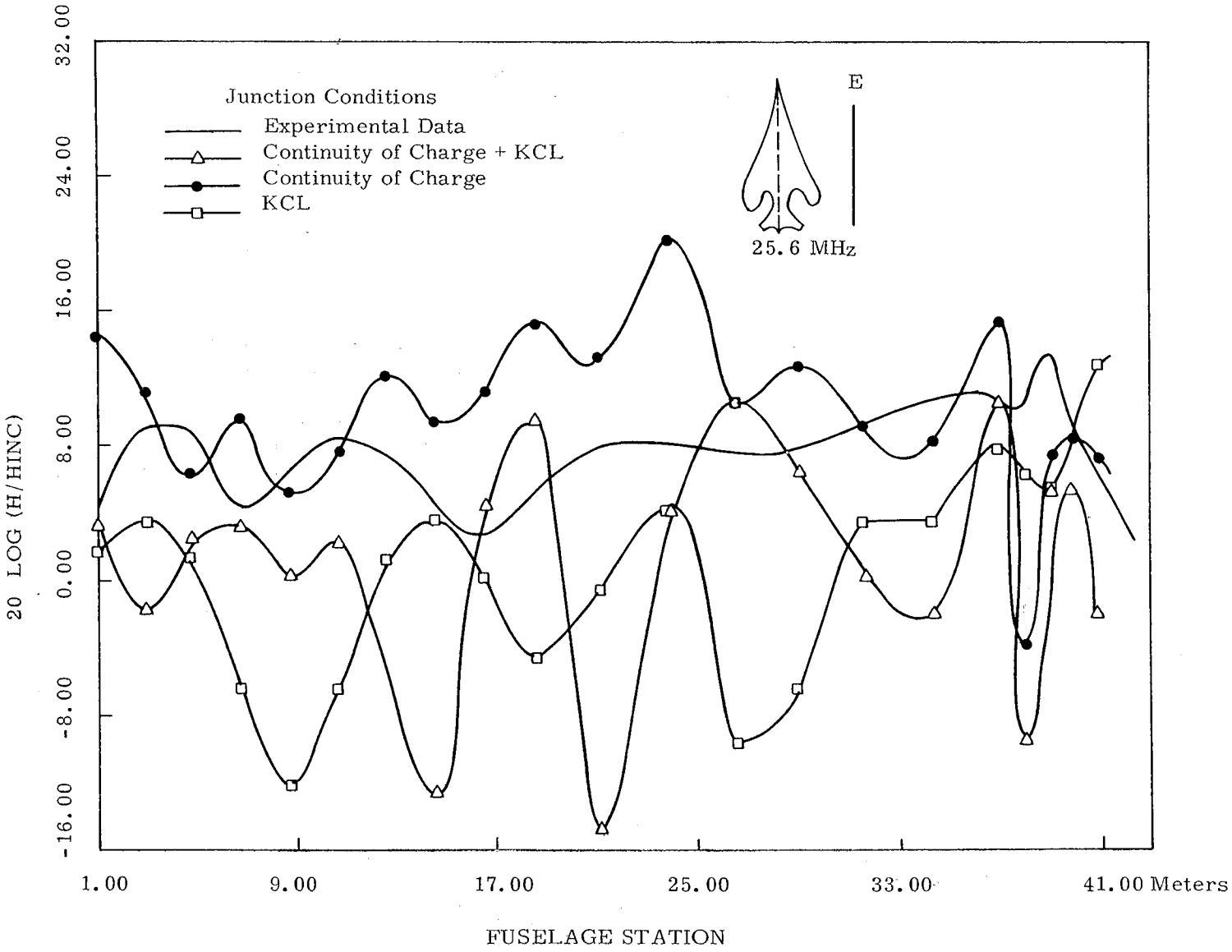

Figure 18: Comparison of B-1 Model Measurements with Wire Model Results (Top-side Incidence)

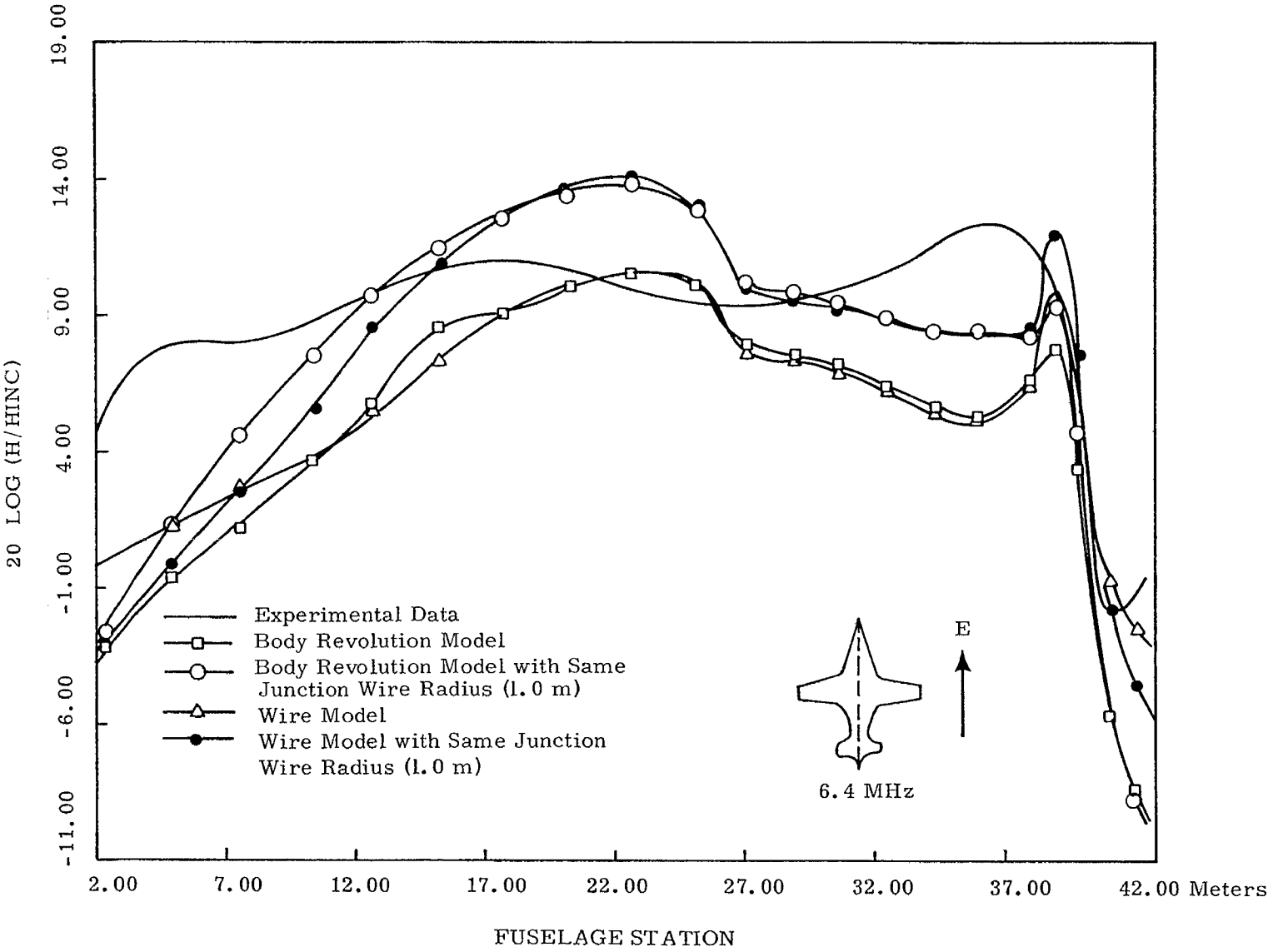

Figure 19: Comparison of B-1 Model Measurements with Results from the Wire Model and the Body of Revolution Model (Top-side incidence)

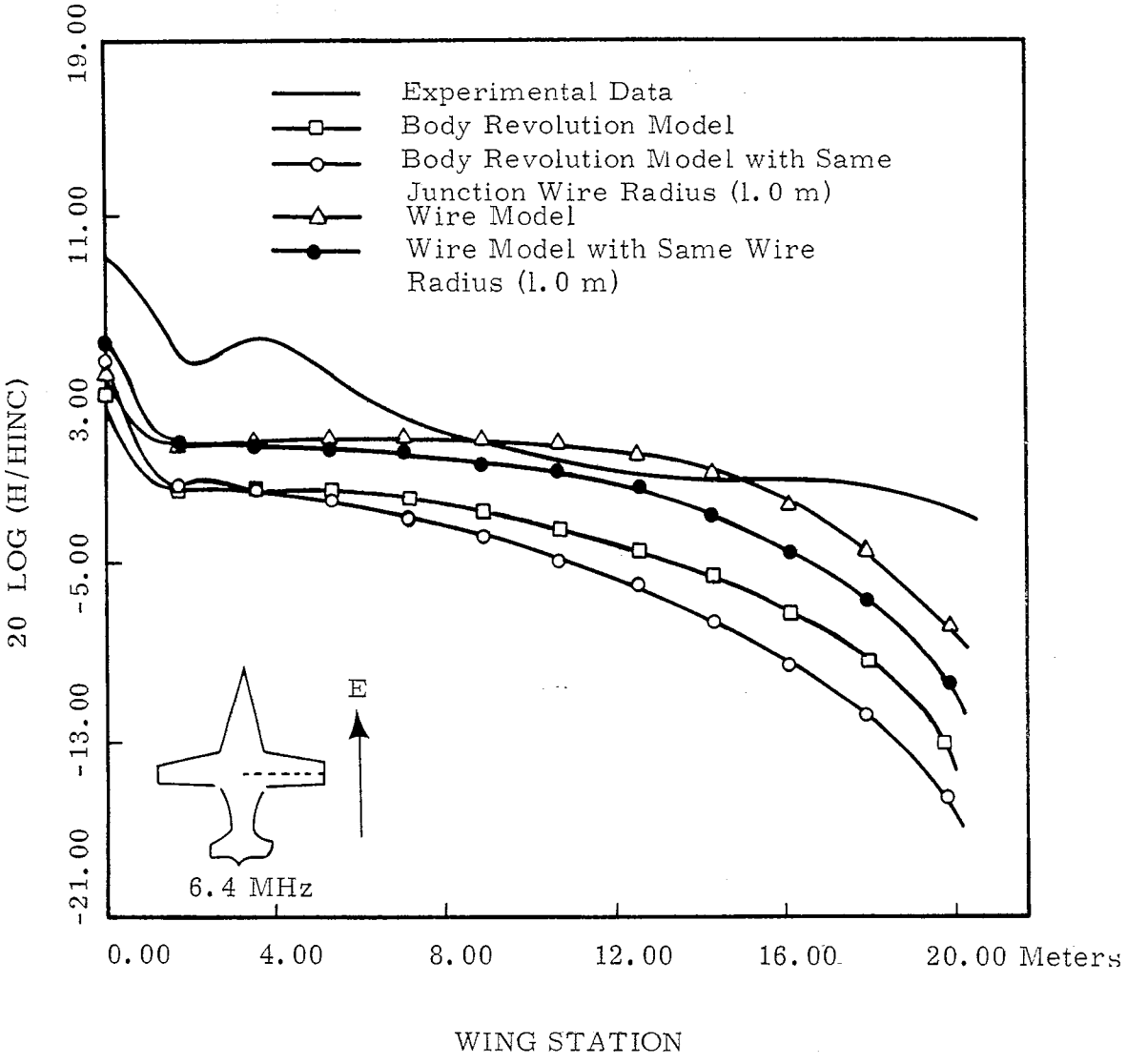

Figure 20: Comparison of B-1 Model Measurements with Results from the Wire Model and the Body of Revolution Model (Top-side Incidence)

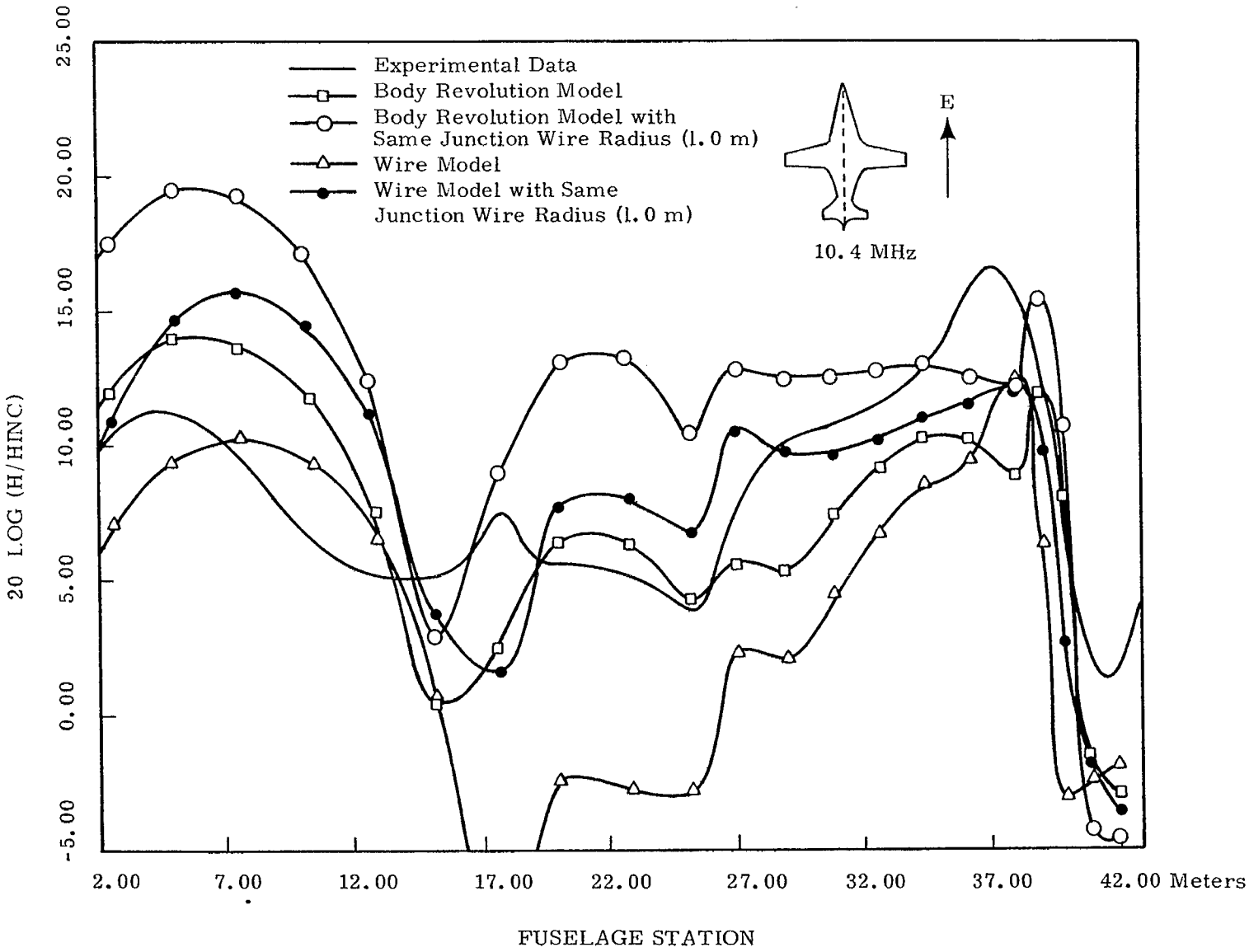

Figure 21: Comparison of B-1 Model Measurements with Results from the Wire Model and the Body of Revolution Model (Top-side Incidence)

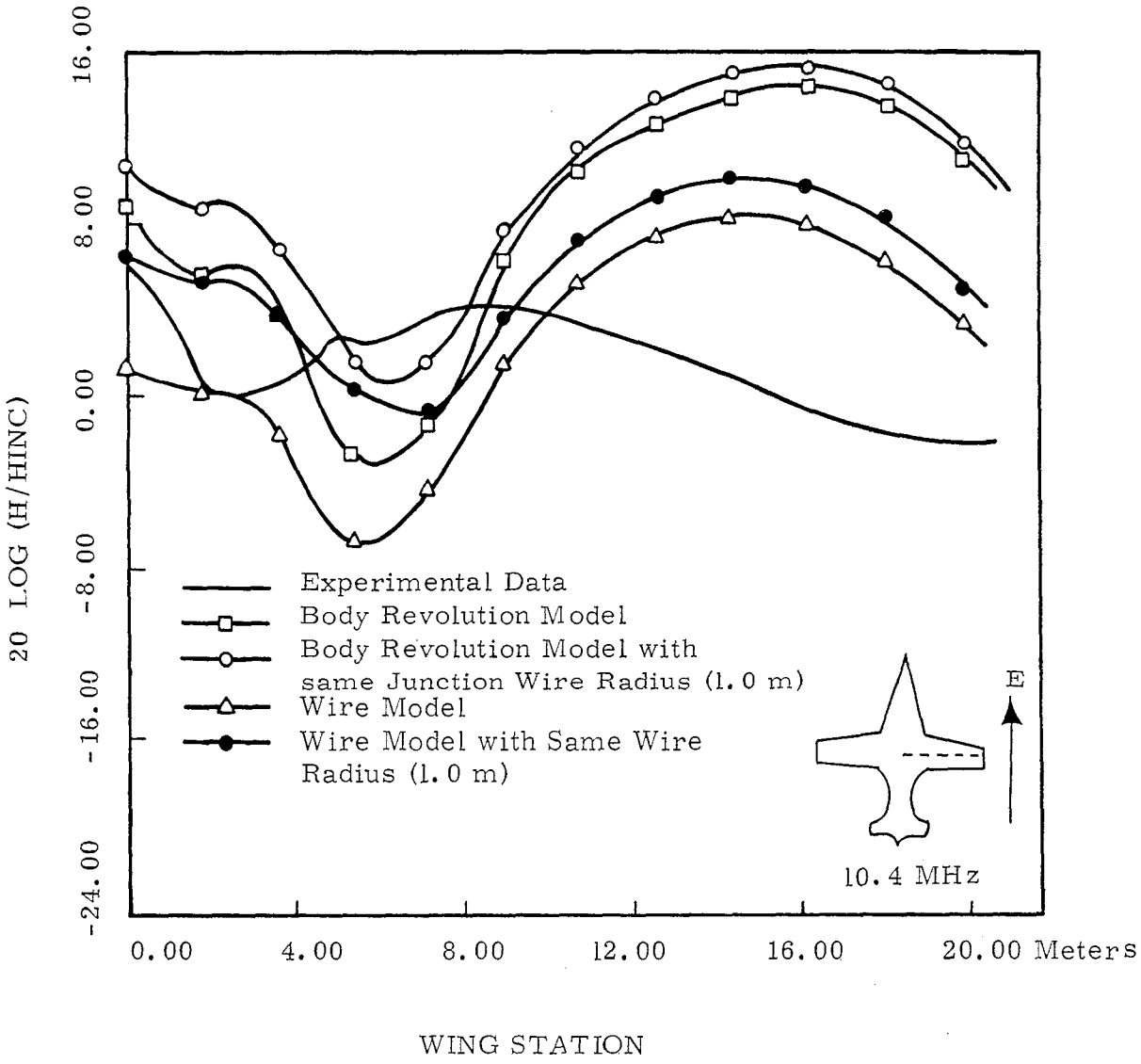

Figure 22: Comparison of B-1 Model Measurements with Results from the Wire Model and the Body of Revolution Model (Top-side Incidence)

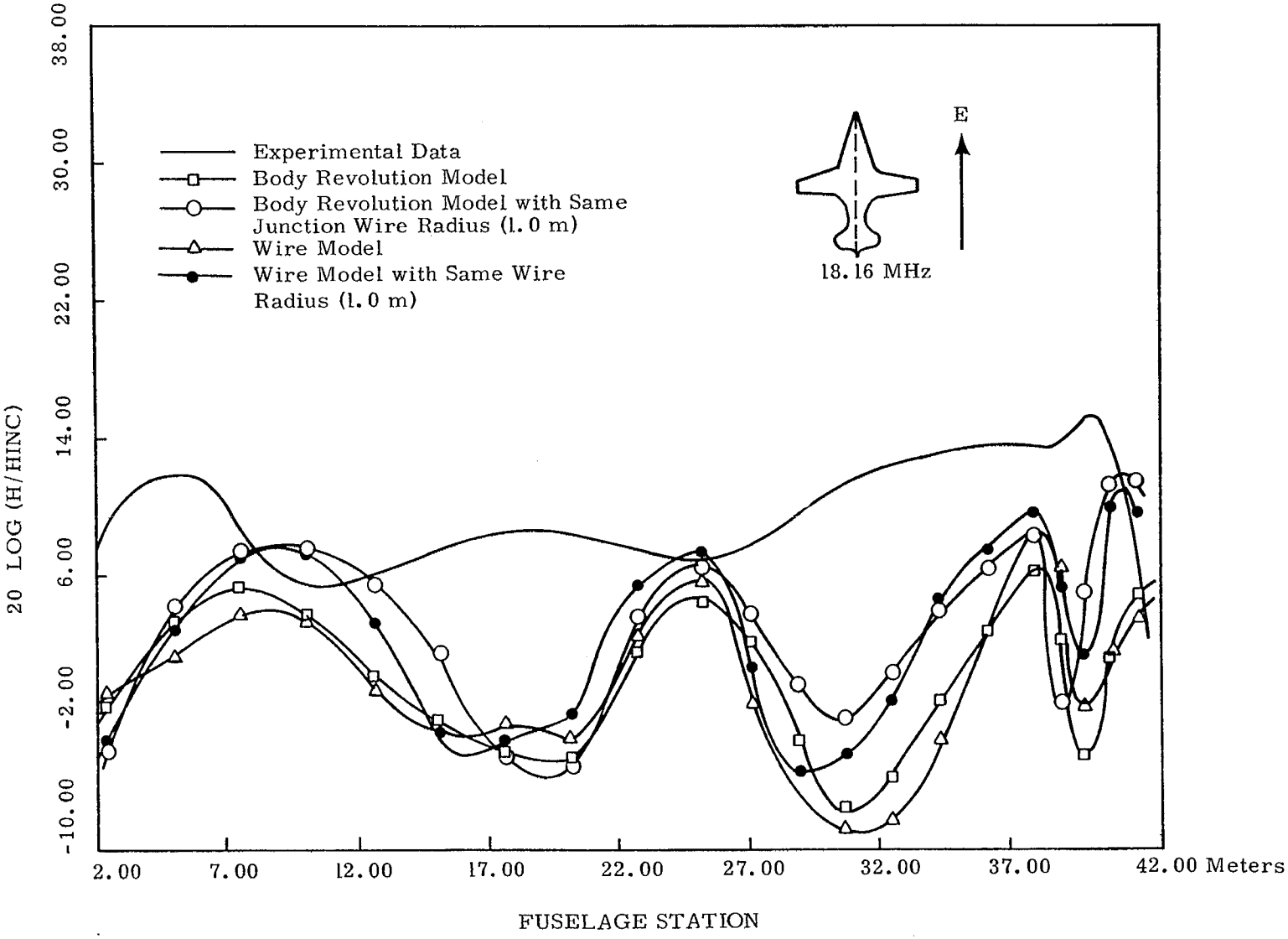

Figure 23: Comparison of B-1 Model Measurements with Results from the Wire Model and the Body of Revolution Model (Top-side Incidence)

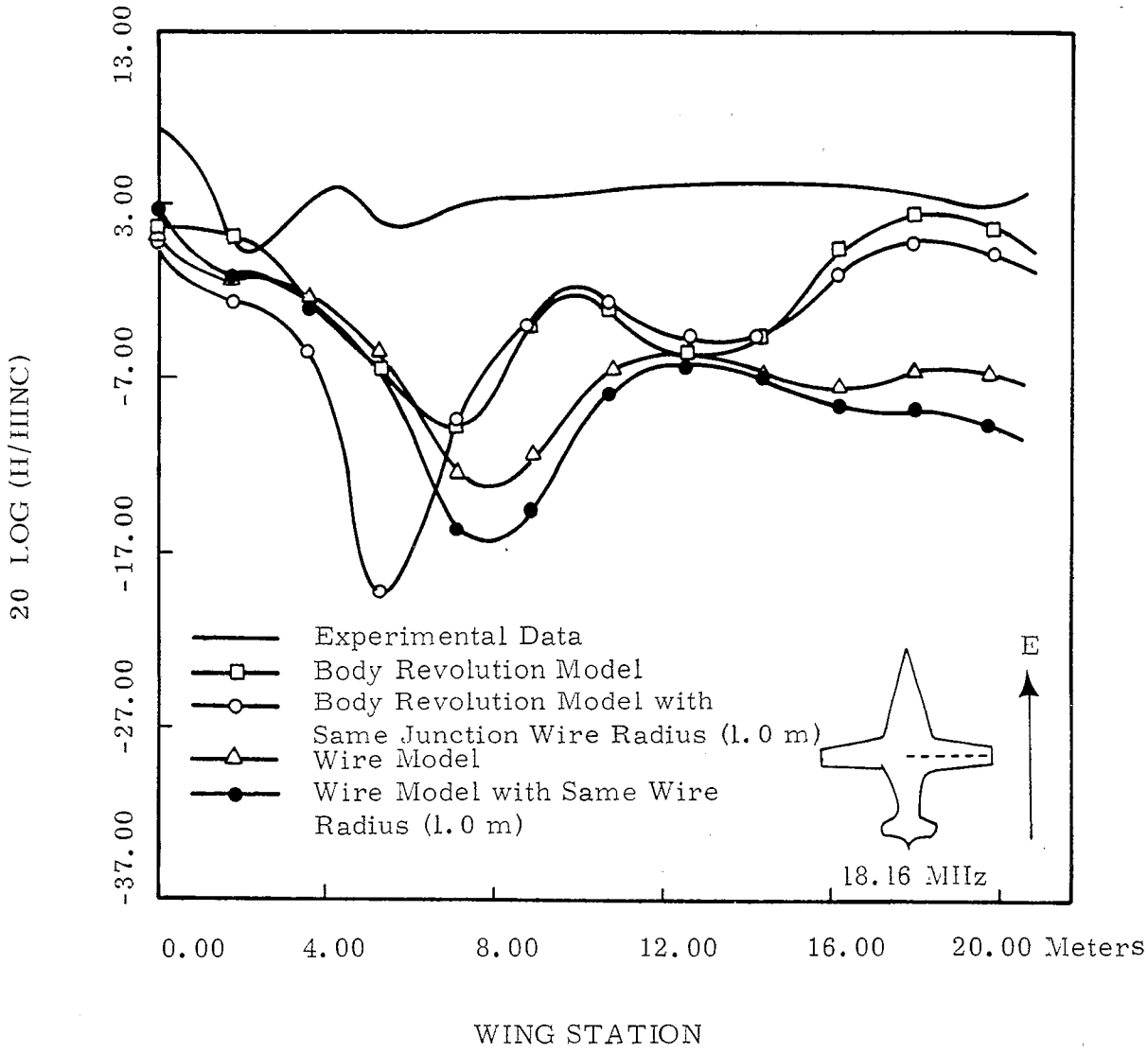

Figure 24: Comparison of B-1 Model Measurements with Results from the Wire Model and the Body of Revolution Model (Top-side Incidence)

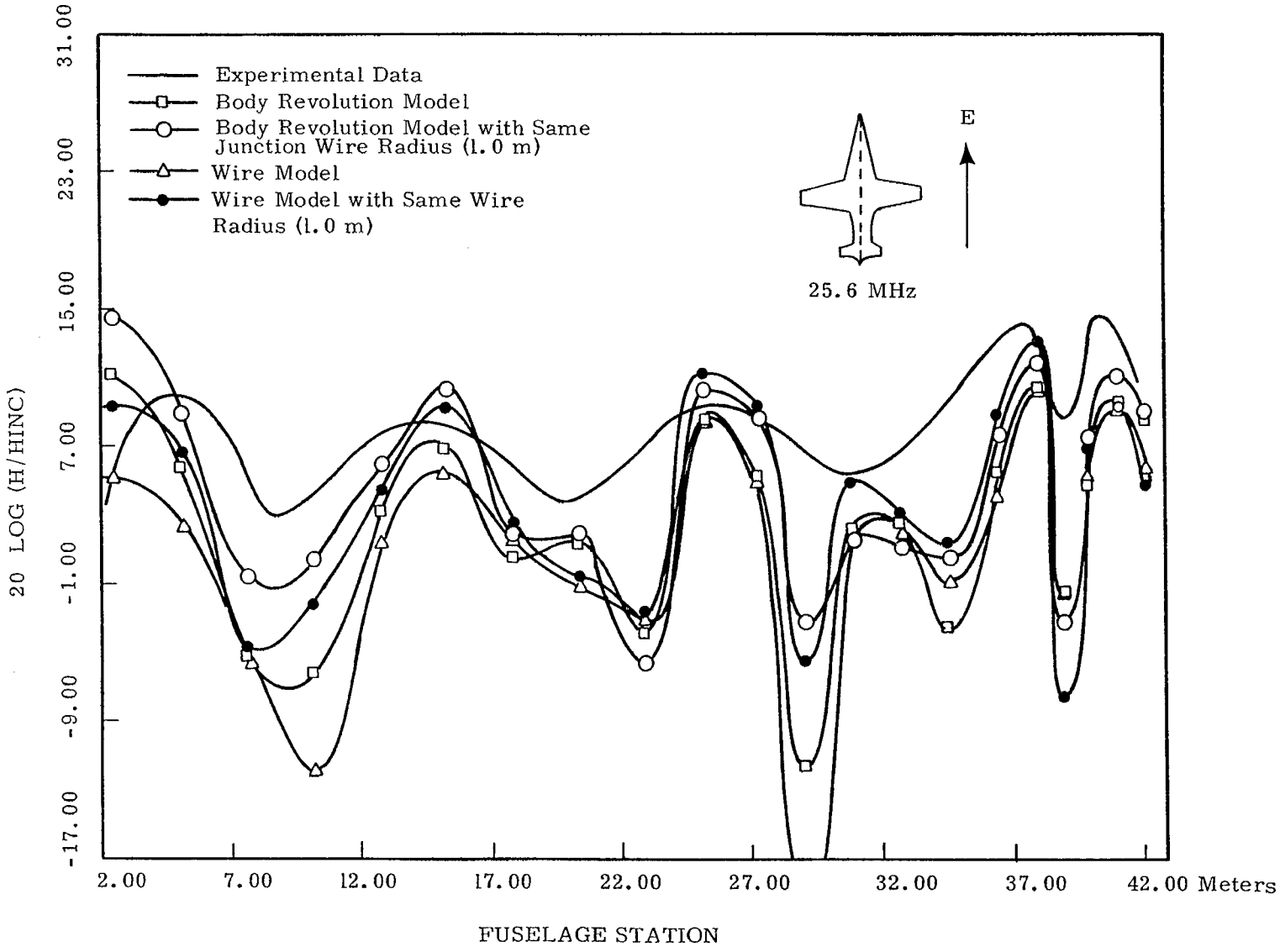

Figure 25: Comparison of B-1 Model Measurements with Results from the Wire Model and the Body of Revolution Model (Top-side Incidence)

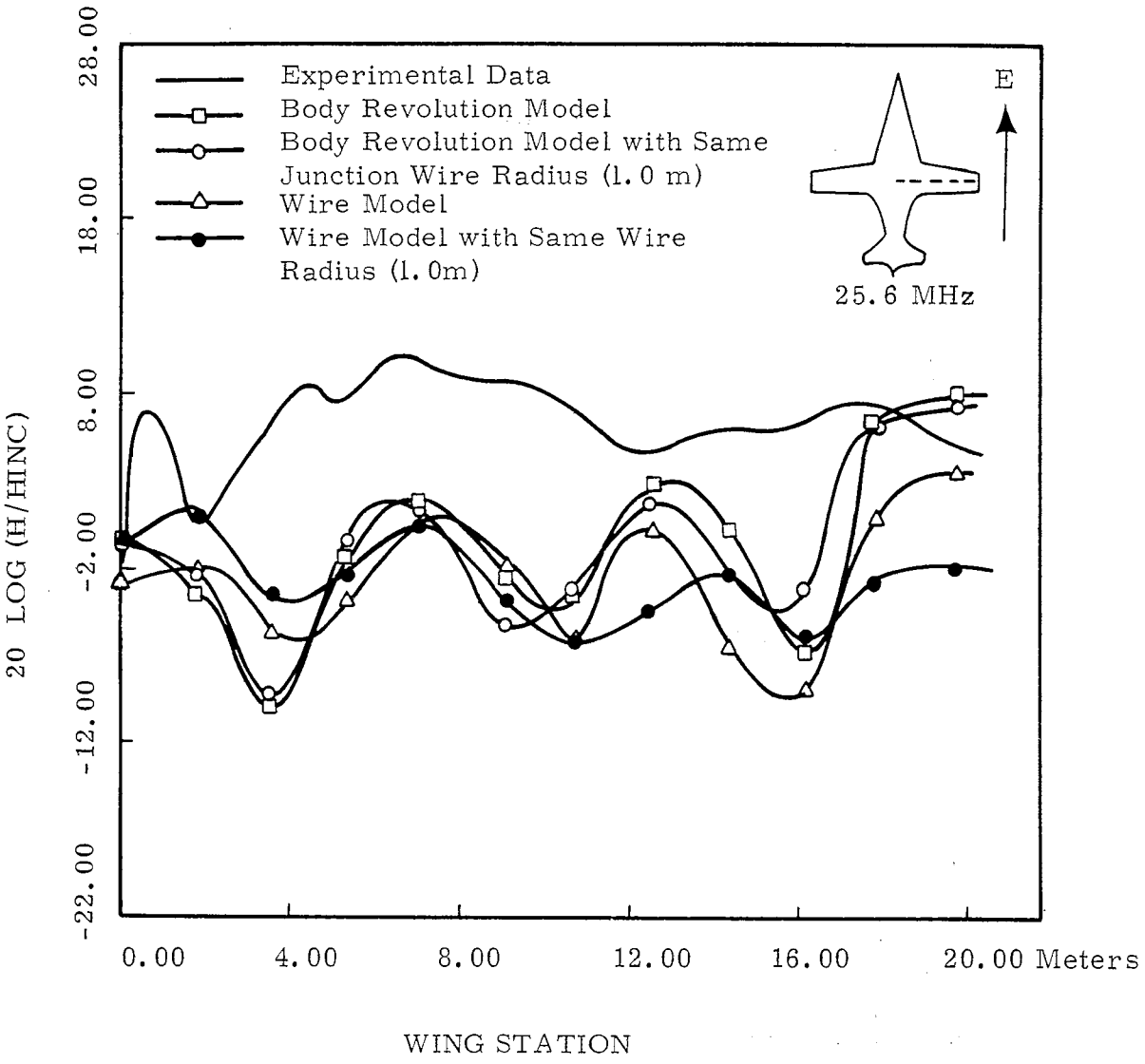

Figure 26: Comparison of B-1 Model Measurements with Results from the Wire Model and the Body of Revolution Model (Top-side Incidence)

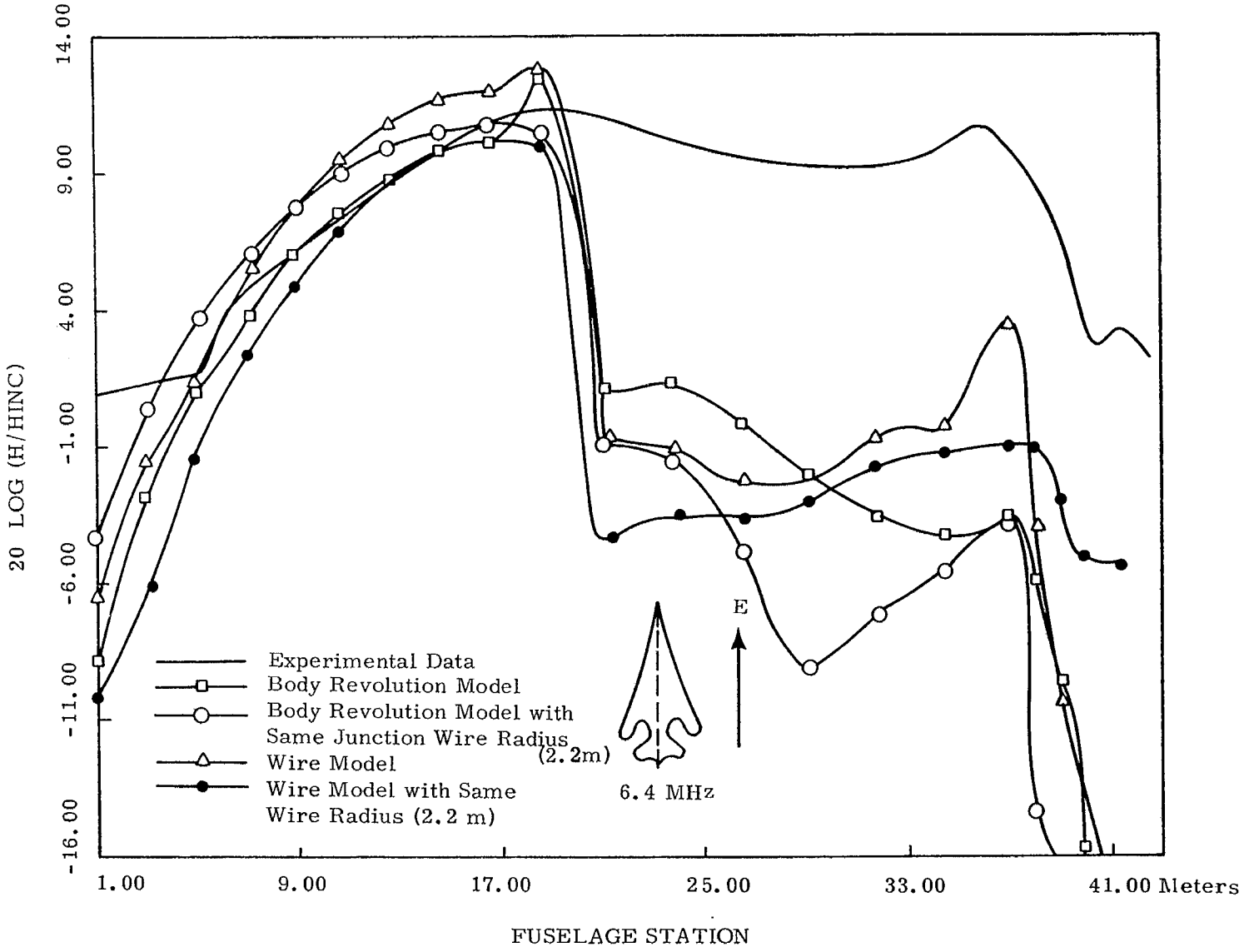

Figure 27: Comparison of B-1 Model Measurements with Results from the Wire Model and the body of Revolution Model (Top-side Incidence)

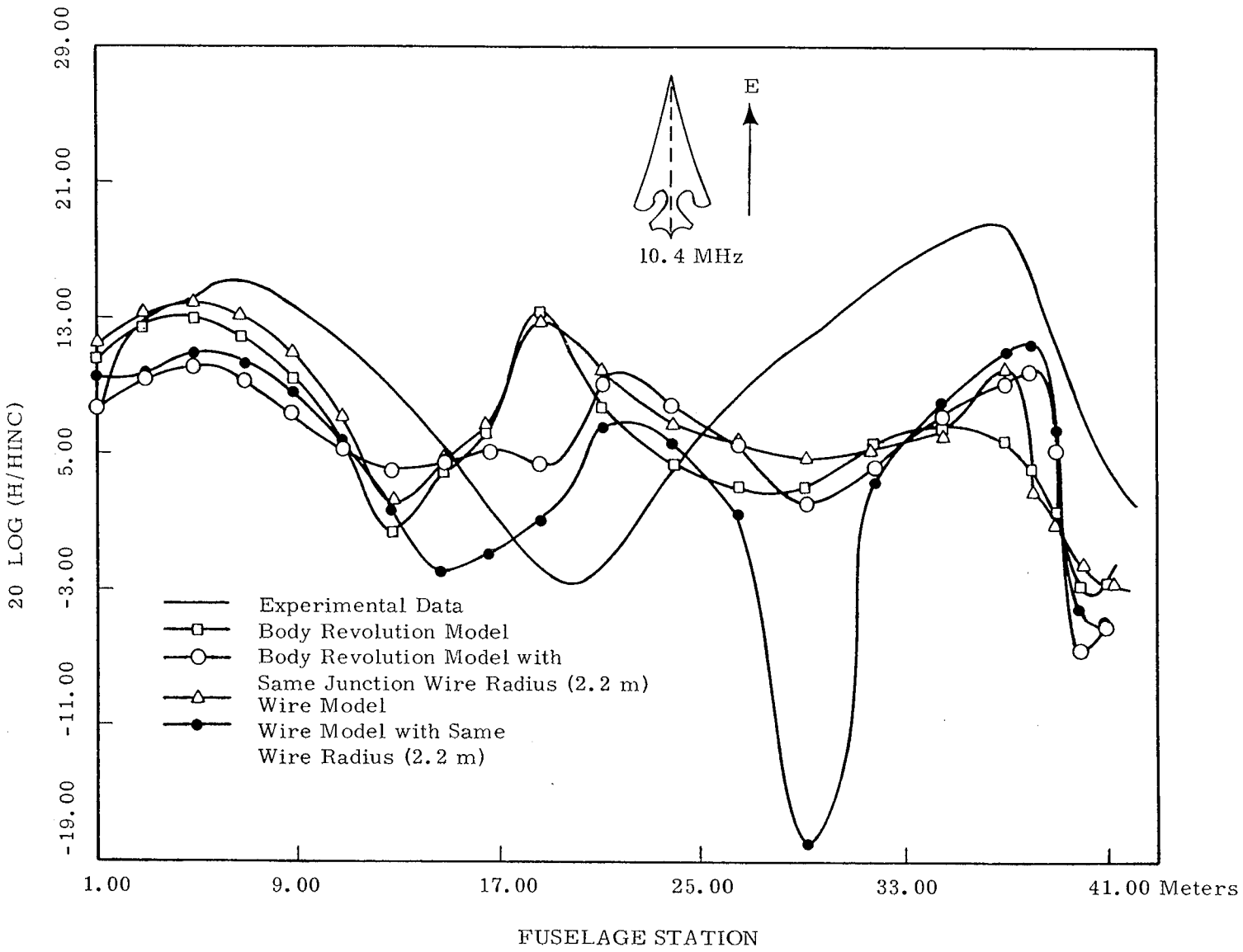

Figure 28: Comparison of B-1 Model Measurements with Results from the Wire Model and the body of Revolution Model (Top-side Incidence)

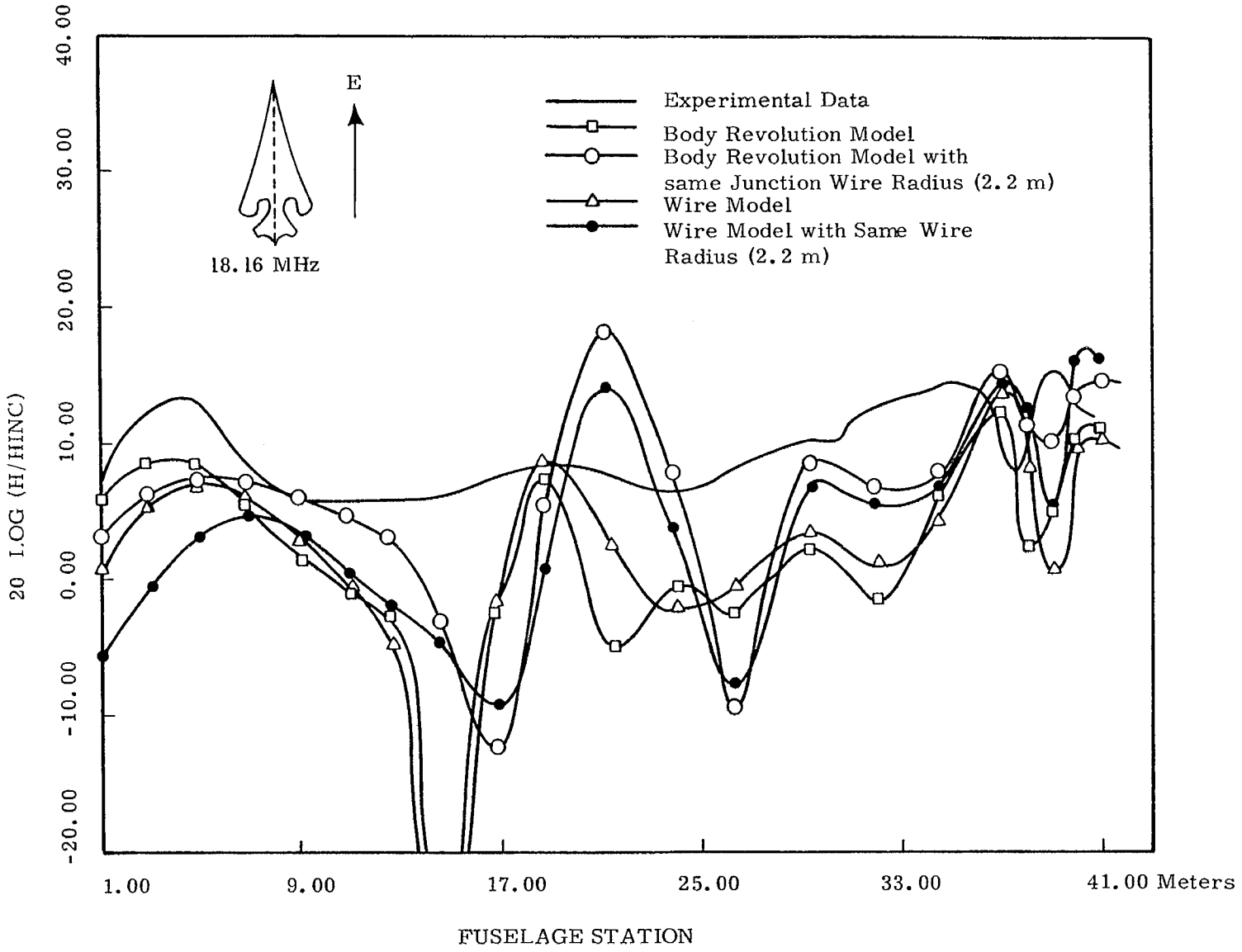

Figure 29: Comparison of B-1 Model Measurements with Results from the Wire Model and the Body of Revolution Model (Top-side Incidence)

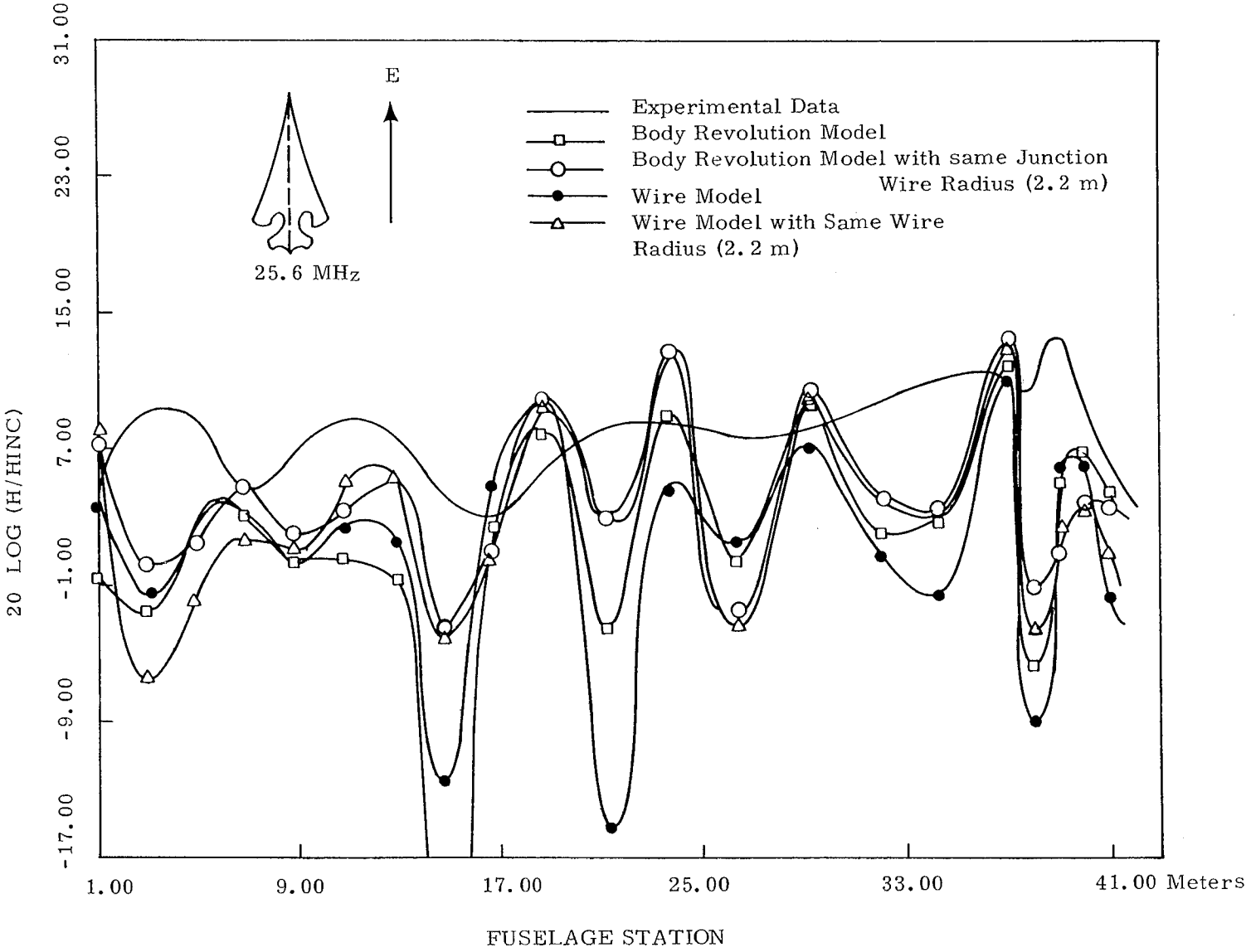

Figure 30: Comparison of B-1 Model Measurements with Results from the Wire Model and the Body of Revolution Model (Top-side Incidence)

frequencies so that the resonant cases could be determined. Due to a low frequency limitation in their source instrumentation 6.4 mHz was the lowest resonant frequency observed, which however is not the lowest resonant frequency and is probably an antiresonant frequency as the investigators suspected (ref.10). Following their procedure for determining resonant frequencies the body of revolution data is also used to determine the resonant frequencies of the B-1 aircraft. These are shown in Table 1.

TABLE 1: Resonant and Antiresonant Frequencies for the B-1 Aircraft with Wings Swept

No.	Resonant Frequencies	
	Model Measurement	Body of Revolution Code
1	-	3.4 mHz
2	10.4 mHz	10.5 mHz
3	18.2 mHz	16.7 mHz
4	25.6 mHz	
	Antiresonant Frequencies	
1	6.4 mHz	6.0 mHz

These resonant frequencies are clearly exhibited in figure 31, where the axial current in the vicinity of the cockpit is plotted versus the frequency of excitation.

2. COMPARISON WITH OTHER THEORETICAL RESULTS

Other electromagnetic models for aircraft have been used to determine skin currents induced by an incident field. Two examples are illustrated in figures 32 and 33. First is the so-called fat cylinder model developed by a group at North American Rockwell International Autonetics

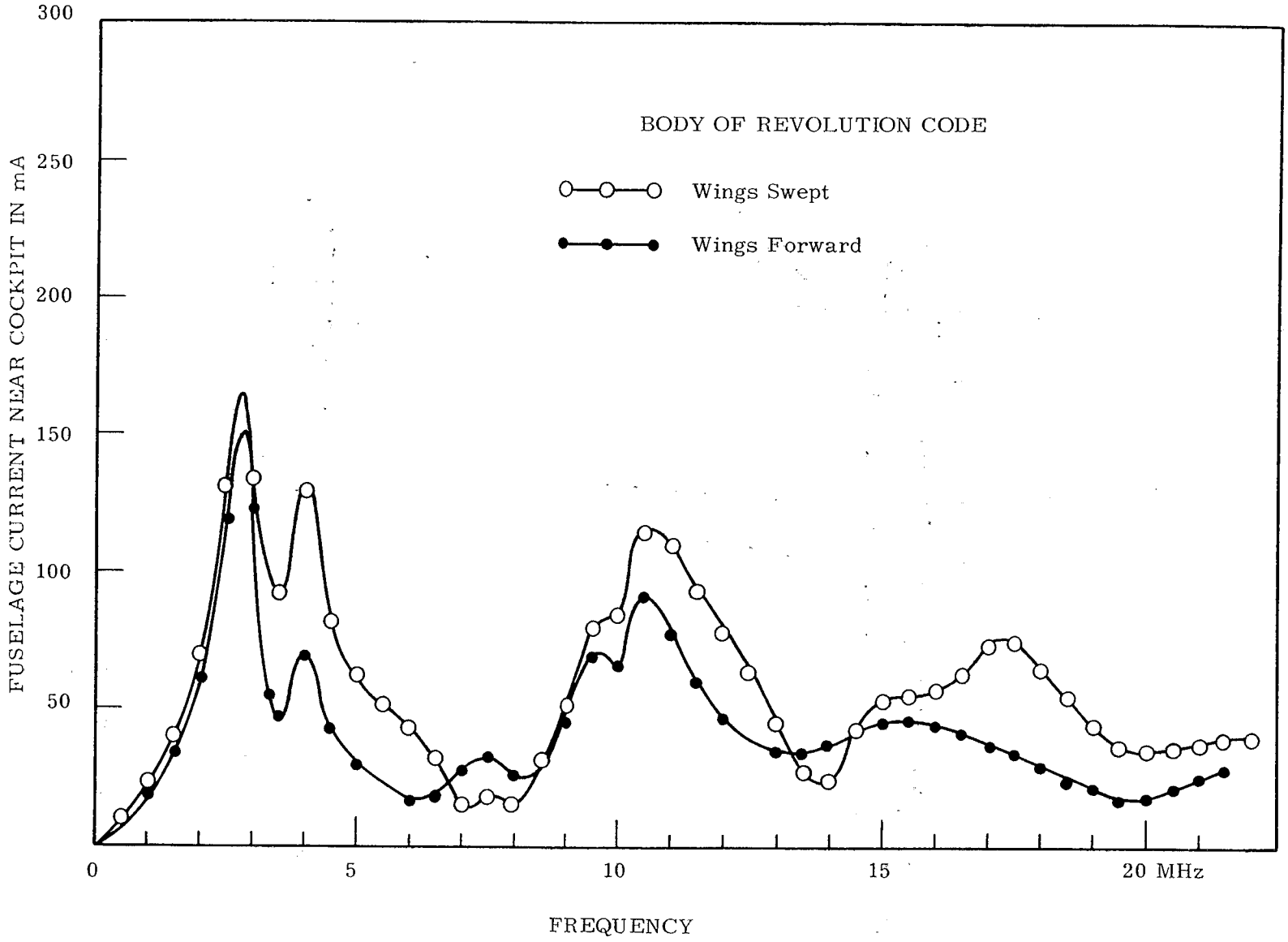

Figure 31. Fuselage Current on the B-1 Aircraft at Body Station 5 (Near the Cockpit) Versus Frequency

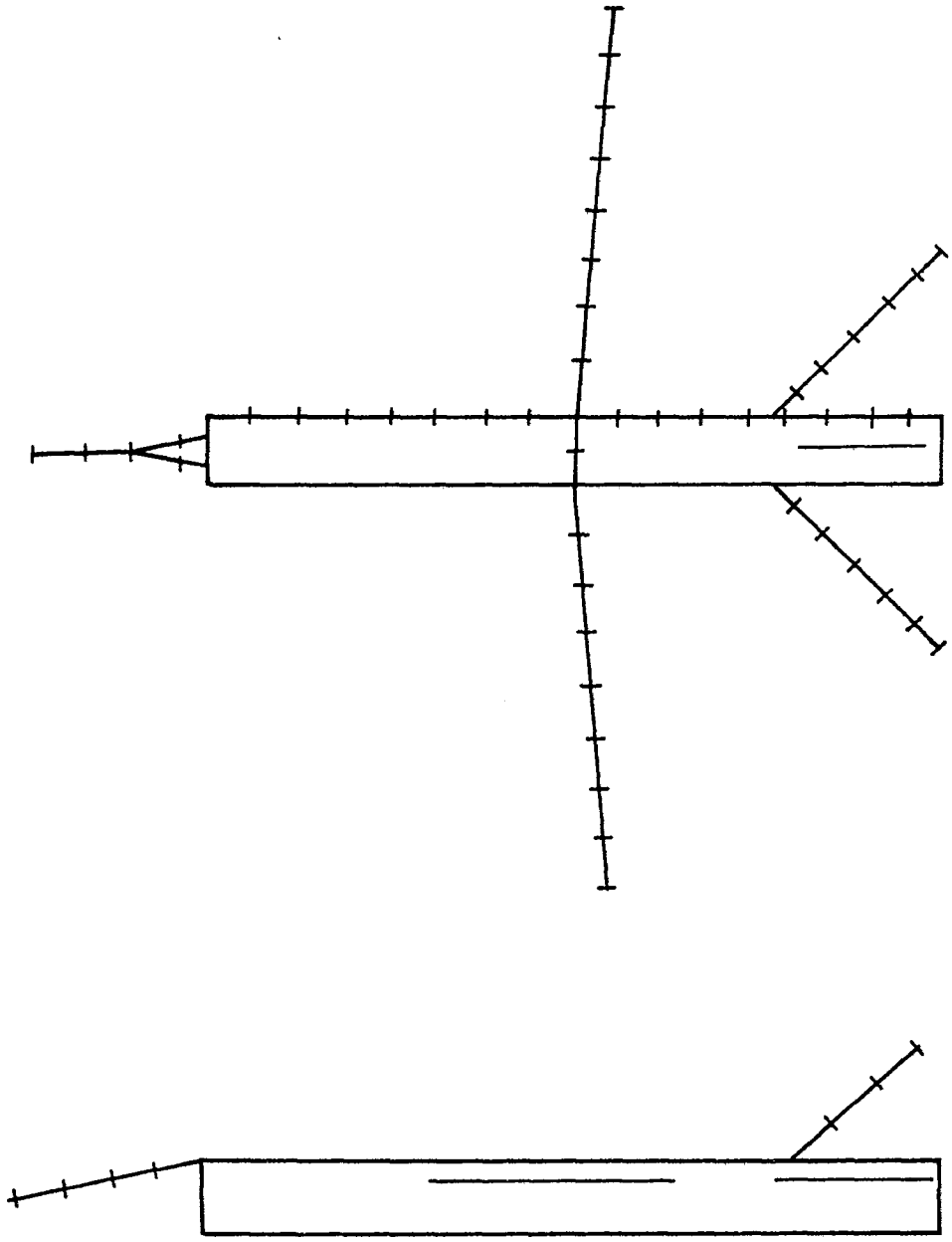

Figure 32: Wire Model Developed at Autonetics for the F-111 Aircraft

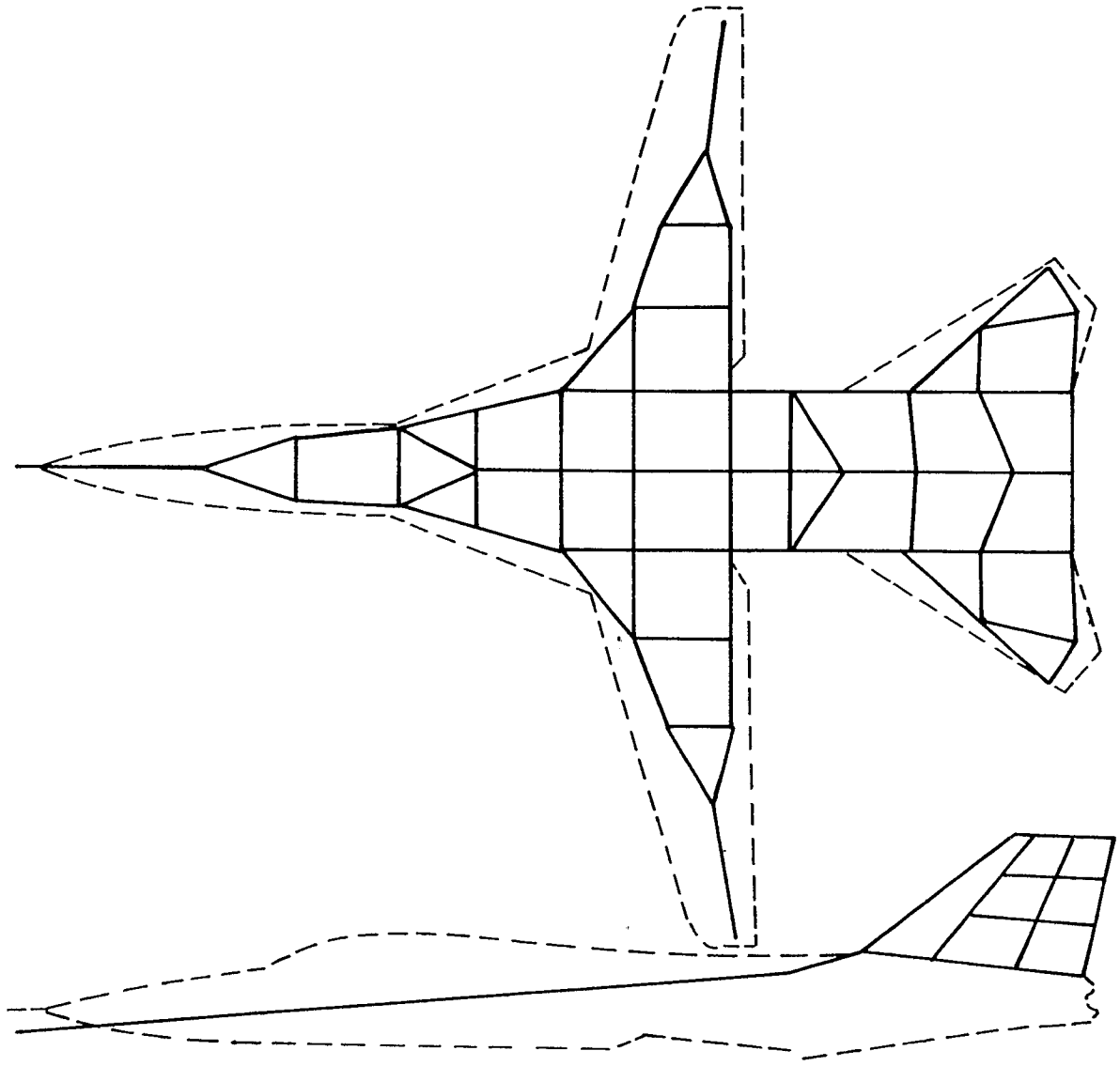

Figure 33: Wire Grid Model Developed at the Boeing Company for the B-1 Aircraft

division. Second is the wire mesh model developed at the Boeing Company, Seattle, Washington. Results obtained for these models are shown in figure 34. These data are given specifically for the F-111 aircraft, roughly a 1/2 scale model of the B-1 aircraft. To compare with the F-111 results the scale model data and the body of revolution data for the B-1 are appropriately scaled. There is a notable difference in the theoretical data. This may be due in part to the points at which the currents are evaluated being different as well as the scaling error. Yet it is difficult to explain why the fat cylinder and the wire mesh models predict nulls at 20 mHz while the scale model measurements and the body of revolution data both indicate resonant peaks in the vicinity of 20 mHz. In any event the comparison is inconclusive.

A perhaps more meaningful comparison is exhibited in figures 35 through 38. Here the wire code generated by Richmond (ref. 20) at Ohio State University is used to model the B-1 aircraft with constant radii cylinders. The obtained current densities are presented for a few typical cases. The agreement between the Richmond computer code results and the body of revolution results is quite reasonable. In particular note the agreement between the Richmond wire code results for the 1.0 meter radius model of figure 37 and the corresponding results for the 1.0 meter case in figure 21.

In the last four figures of the foregoing discussion the discontinuities in the wire currents at the wire junctions are shown in the body of revolution data. Actually these discontinuities occur in all

---

20. Richmond, J. H., "Radiation and Scattering by Thin-Wire Structures in a Homogeneous Conducting Medium," IEEE Trans. Ant. Prop. (Computer program descriptions), Vol. AP-22, p. 365, March 1974.

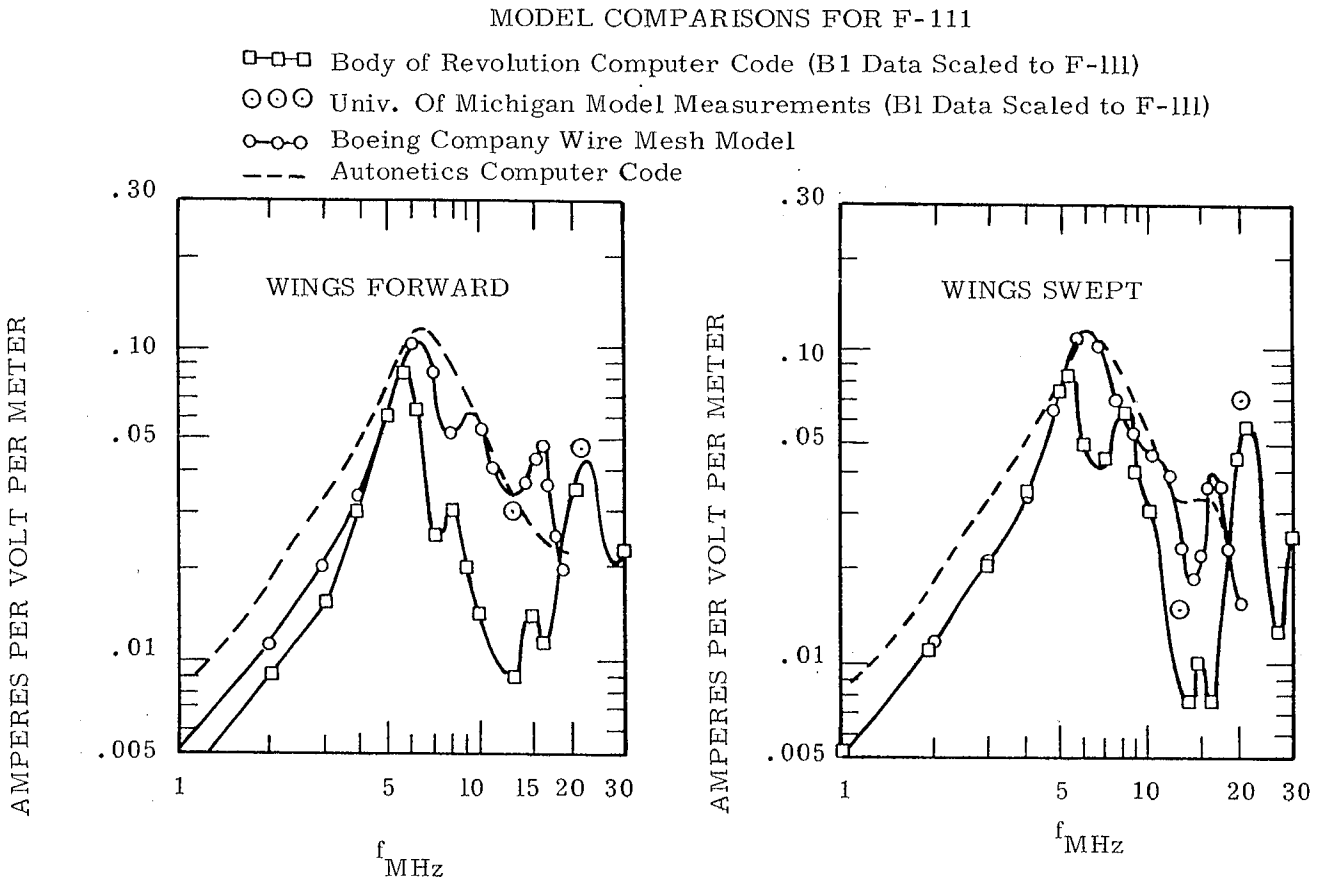

Figure 34: Fuselage Current Near Cockpit for the Incident Electric Field Parallel to Fuselage and Topside Incidence

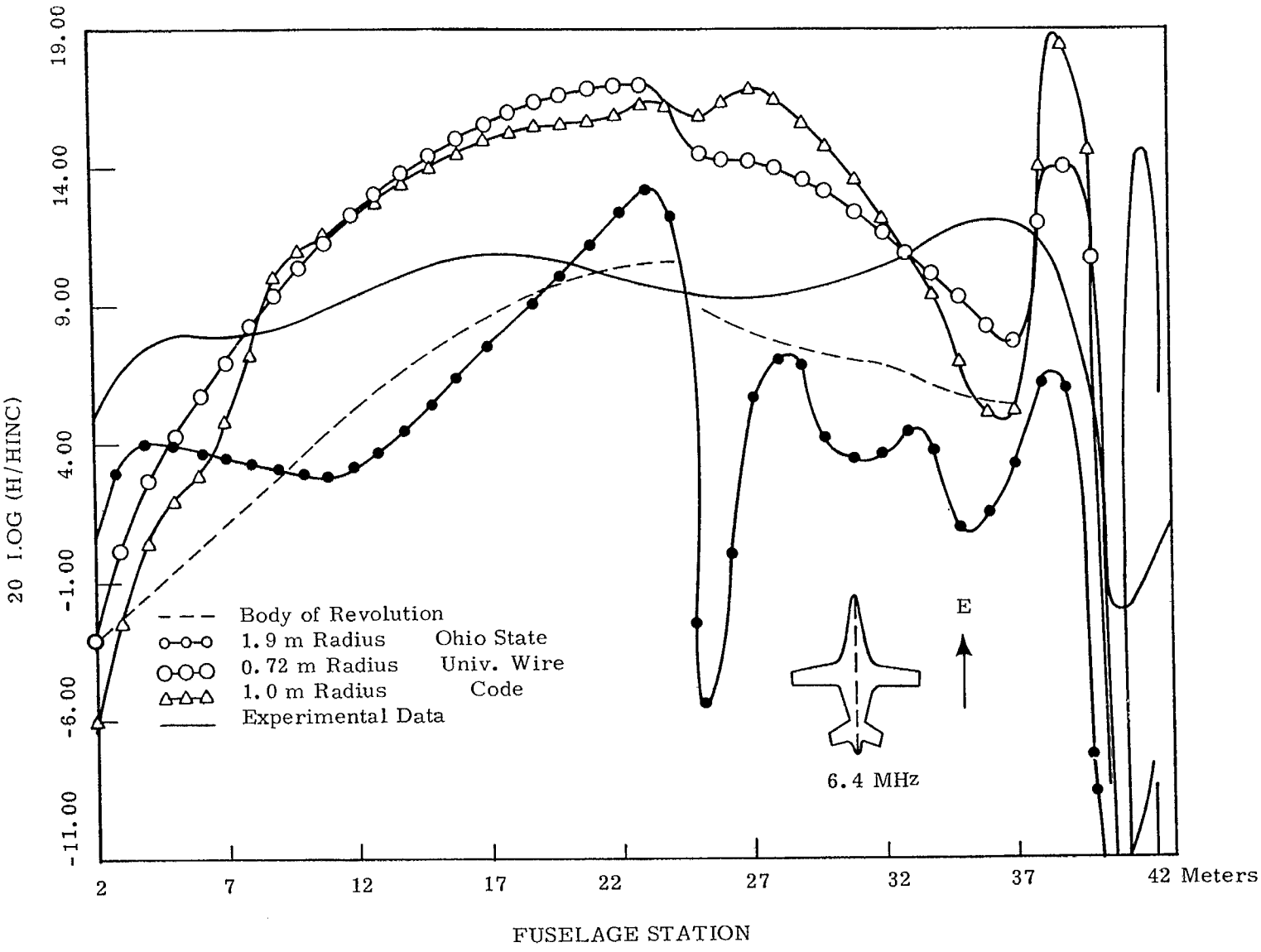

Figure 35: Comparison of the Results from the Body of Revolution Computer Code with the Results from the Ohio State University Wire Code

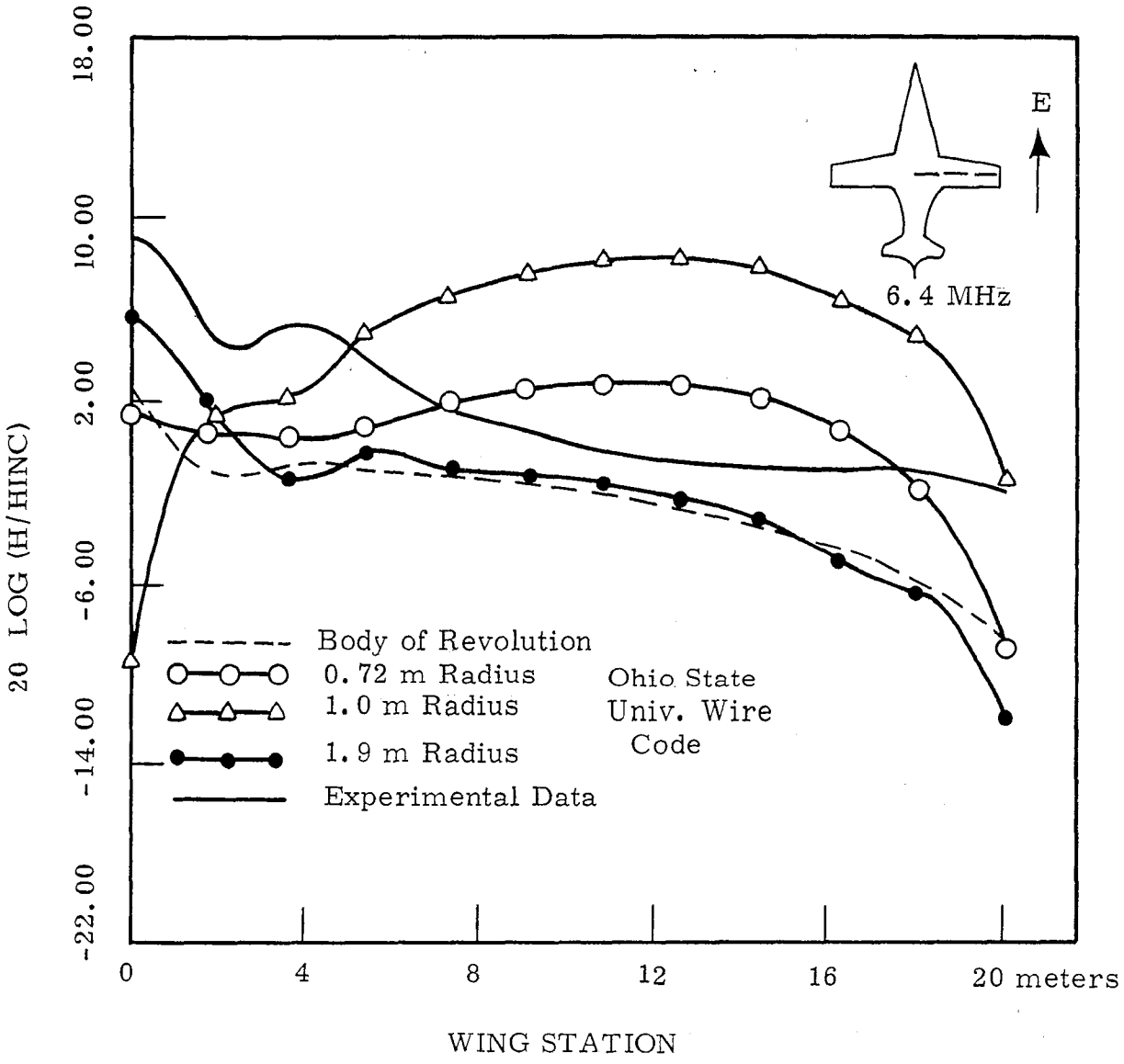

Figure 36: Comparison of the results from the Body of Revolution Computer Code with the Results from the Ohio State Wire Code

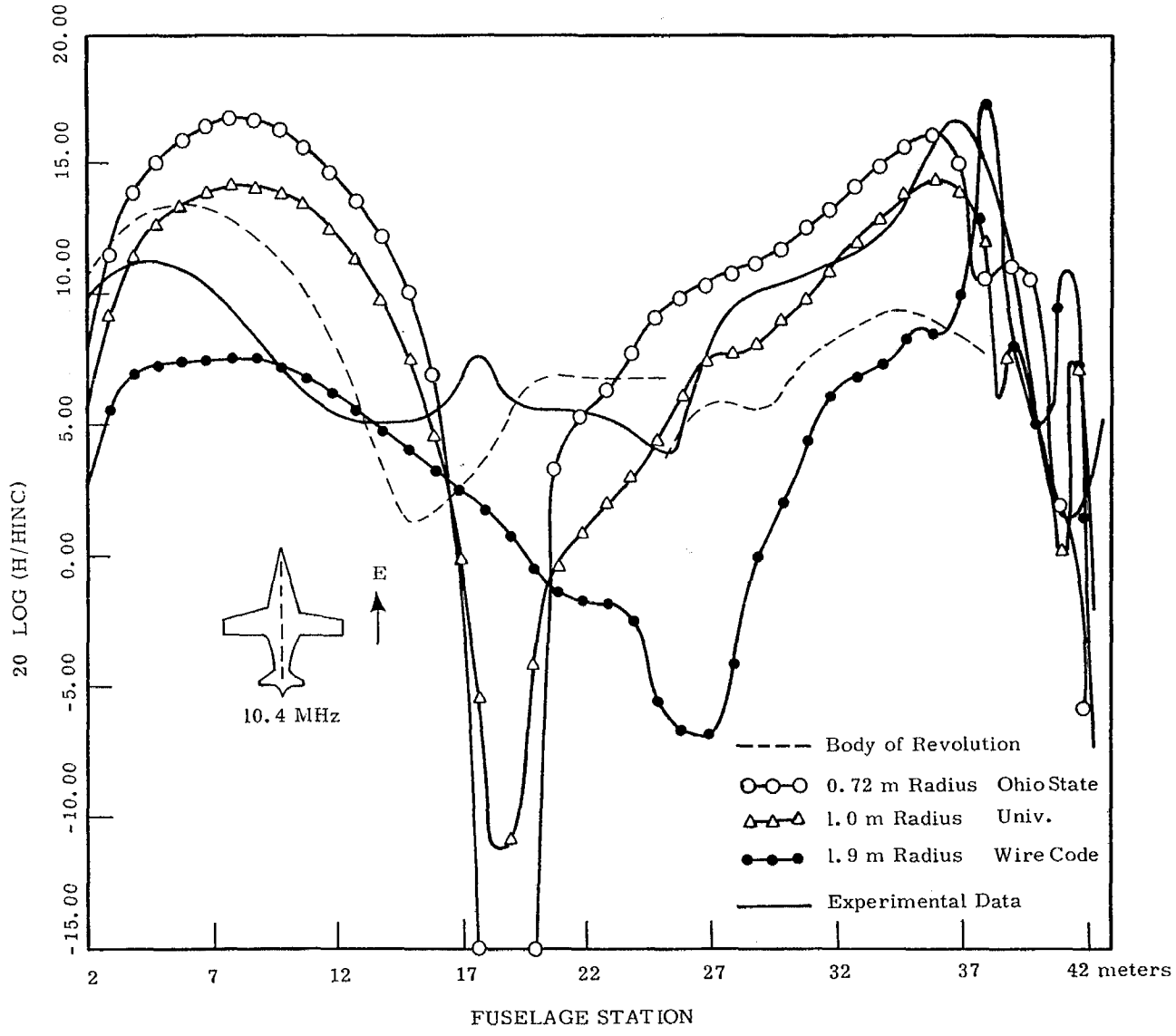

Figure 37: Comparison of the Results from the Body of Revolution Computer Code with the Results from the Ohio State University Wire Code

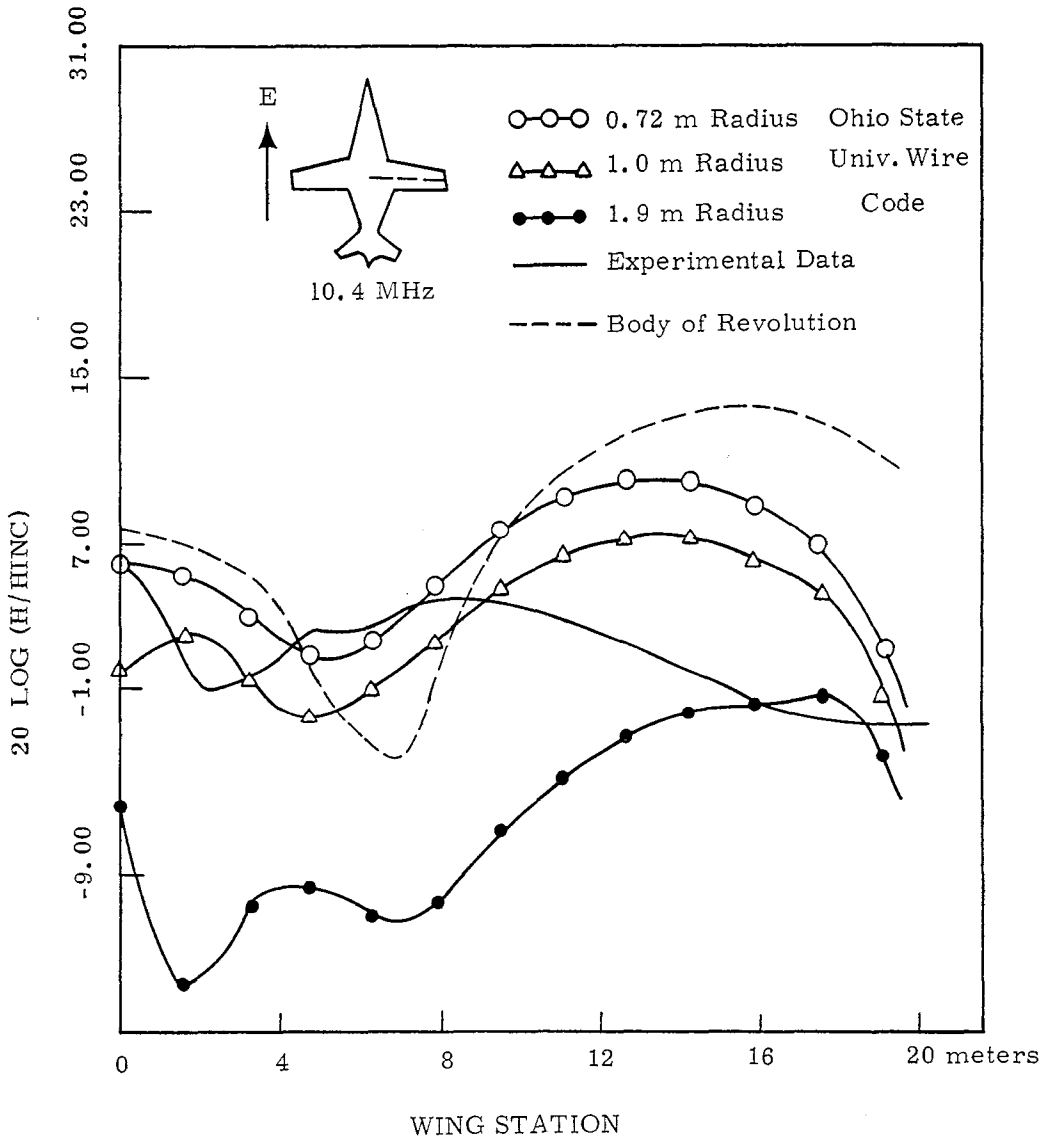

Figure 38: Comparison of the Results from the Body of Revolution Computer Code with the Results from the Ohio State University Wire Code

the previous theoretical data but are not shown explicitly, i.e. the current density data are smoothed through the junction region. It is readily observed that the theoretical predictions for the wings forward configuration agree better with the experimental data than the corresponding predictions for the swept wing configuration. This may be expected for a couple of reasons. First, the junction region for the swept wing case becomes a significant portion of the aircraft structure and thereby certain simplifying assumptions of the theoretical model become questionable. Second, there is a significant overlap of the wings and the fuselage. Thus an appreciable portion of the fuselage supports the wing directed currents. In this overlapping region a superposition of wing and fuselage currents is probably necessary. Carrying out this superposition at the junction points did yield better agreement between the theoretical and experimental data. However, more work is required in this area.

3. SINGULARITY EXPANSION METHOD RESULTS

The singularity expansion method may be applied with considerable advantage to transient scattering problems. In carrying out the solution technique a great deal of insight into the response characteristics of the scattering object is obtained. For example the method yields directly the resonant frequencies of the scattering structure. The details of the computational procedures are given in ref. 8.

In order to determine the induced current and charge induced on a conducting finite sized object it is first necessary to determine the natural frequencies, the simple pole singularities of the Laplace transform of the induced current and charge. Because of the amount of time

available only a few natural frequencies have been obtained. These are exhibited in Table 2.

TABLE 2: Natural Frequencies for the B-1 Aircraft

s/c

Wings Forward	Wings Swept
-0.0039 + j 0.0597	-0.0042 + j 0.0602
-0.0180 + j 0.2066	-0.0271 + j 0.2040

From Table 2 it is seen that in the wings forward configuration the B-1 aircraft resonates at 2.85 and 9.86 mHz and in the wings swept configuration the resonant frequencies are 2.87 and 9.74 mHz. These are in excellent agreement with the model measurements reported in the foregoing.

4. GROUND ALERT CALCULATIONS

The presence of the ground plane results in the incident field being reflected back onto the aircraft with a 180° phase shift in the component of the electric field parallel to the ground that is also parallel to the wings and fuselage of the aircraft. This reflection along with the nearness of the aircraft to the ground tends to remove some of the low frequency content of the pulse illumination. For an incident pulse that is propagating normal to the ground the Laplace transform of the electric field (incident + reflected) at a height h is

$$E_h(s) = E^{inc}(s)[1 + \Gamma(s)e^{-s2h/c}] \qquad (17)$$

where $E^{inc}(s)$ is the Laplace transform of the incident pulse and $\Gamma(s)$ is the reflection coefficient of the ground. If the ground is perfectly conducting then

$$\Gamma(s) = -1$$

Thus it is immediately seen from eqn. (17) that the reflection process eliminates a significant portion of the low frequency content of the incident pulse.

Another effect of the ground is the formation of high Q transmission lines. The wings and fuselage being parallel to the ground will have electromagnetic images in the ground that are mutually parallel to the wings and fuselage thus forming sets of two wire transmission lines. These transmission lines will resonate at about the same frequencies as the aircraft in free space but with a higher Q. However, the Q factor does depend upon the ground conductivity and the resonant frequencies. Of course as the frequency increases the induced current and charge in the ground alert mode become more like those induced in the flight mode.

To appreciate the effect of the ground for the ground alert mode figures 39 through 46 present induced fuselage and wing current densities at 6.4, 10.4, 18.16 and 25.6 mHz, with the center of the fuselage 4.1 meters above the ground plane. These data illustrate the aforementioned ground effects. Apparently the body of revolution calculated data is to be preferred.

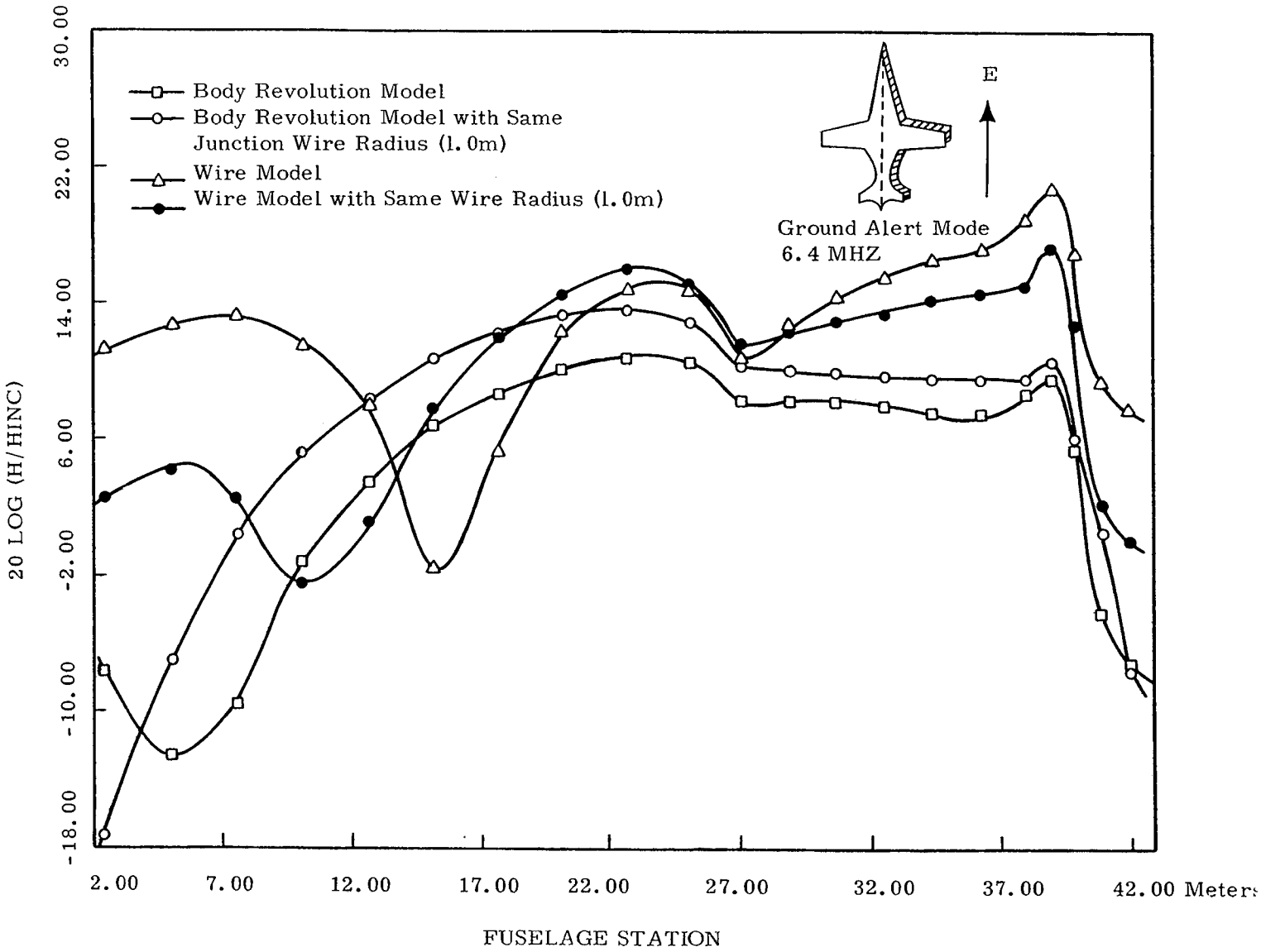

Figure 39: Fuselage Current Density for the B-1 in the Ground Alert Mode with Top-side Incidence, **h = 4.1 Meters**

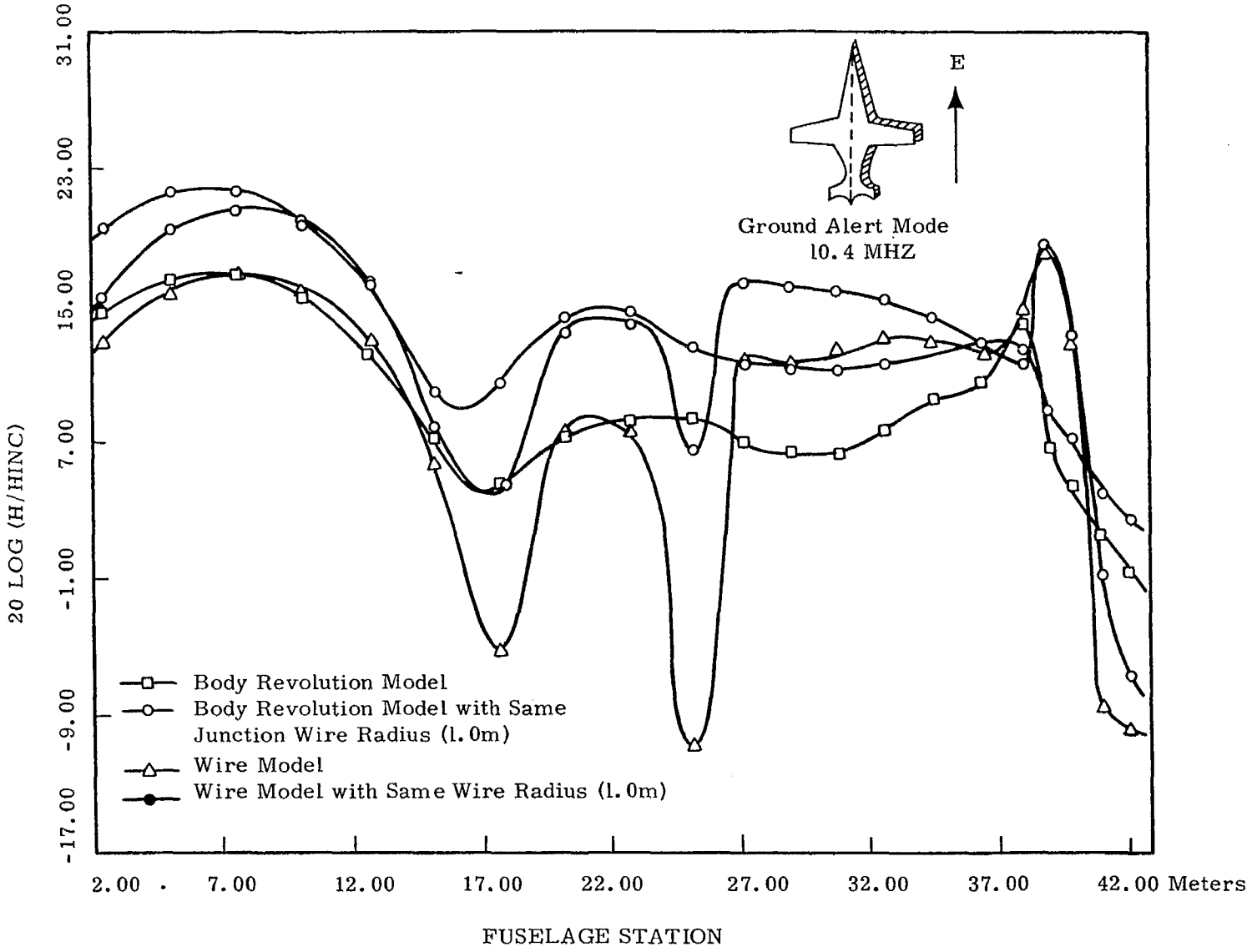

Figure 40: Fuselage Current Density for the B-1 in the Ground Alert Mode with Top-side Incidence, h = 4.1 Meters

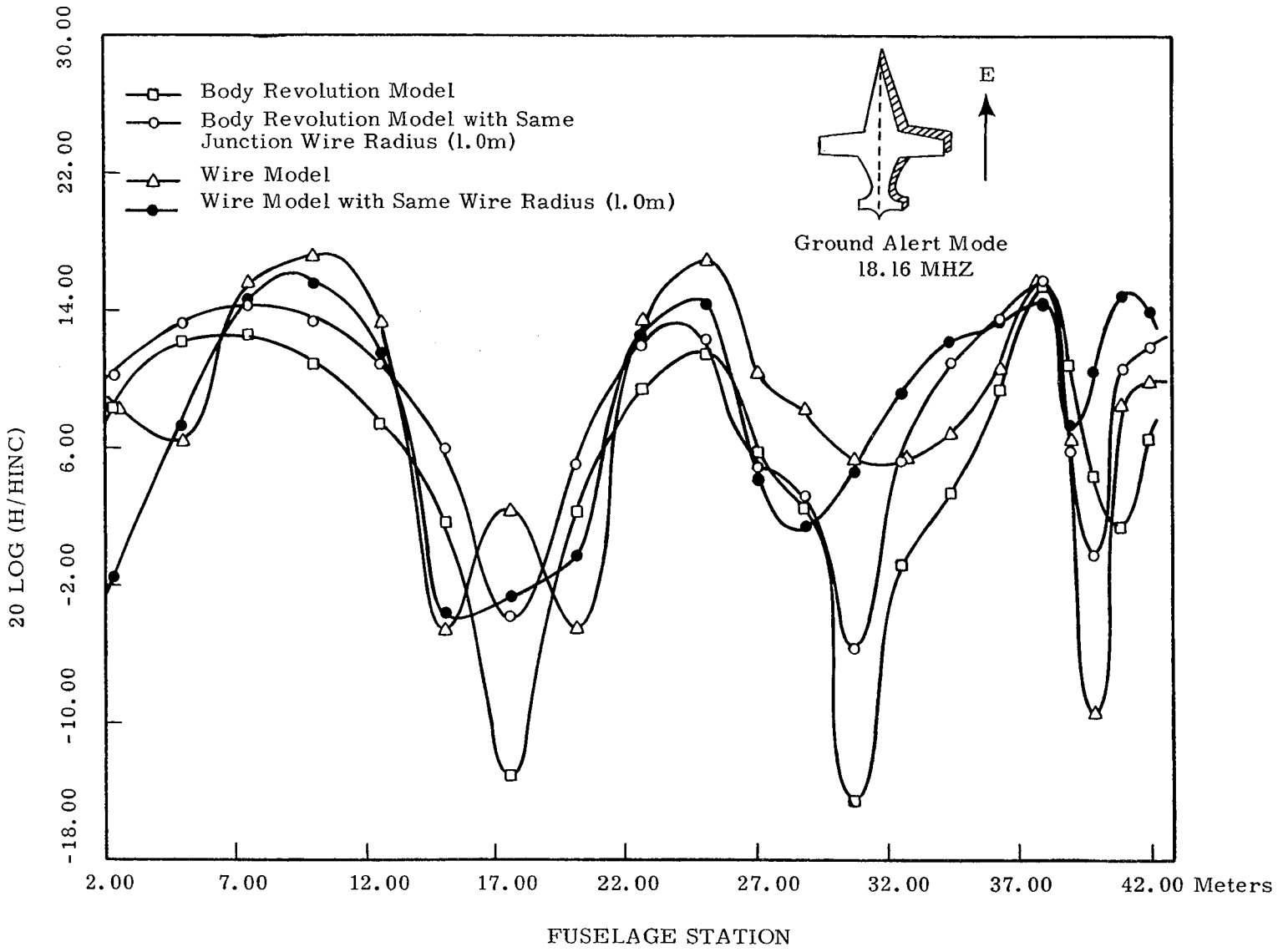

Figure 41: Fuselage Current Density for the B-1 in the Ground Alert Mode with Top-side Incidence, h = 4.1 Meters

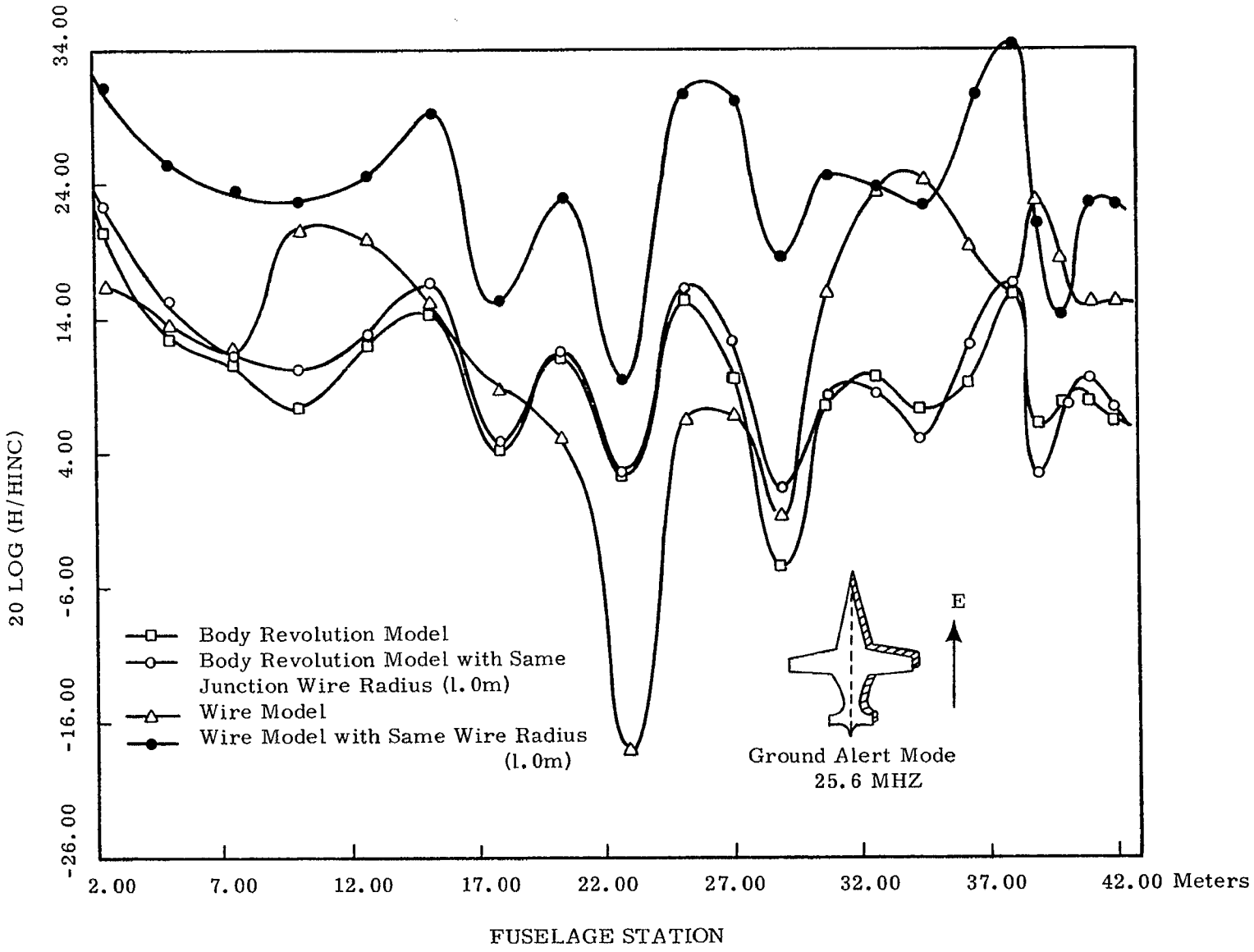

Figure 42: Fuselage Current Density for the B-1 in the Ground Alert Mode with Top-side Incidence, h = 4.1 Meters

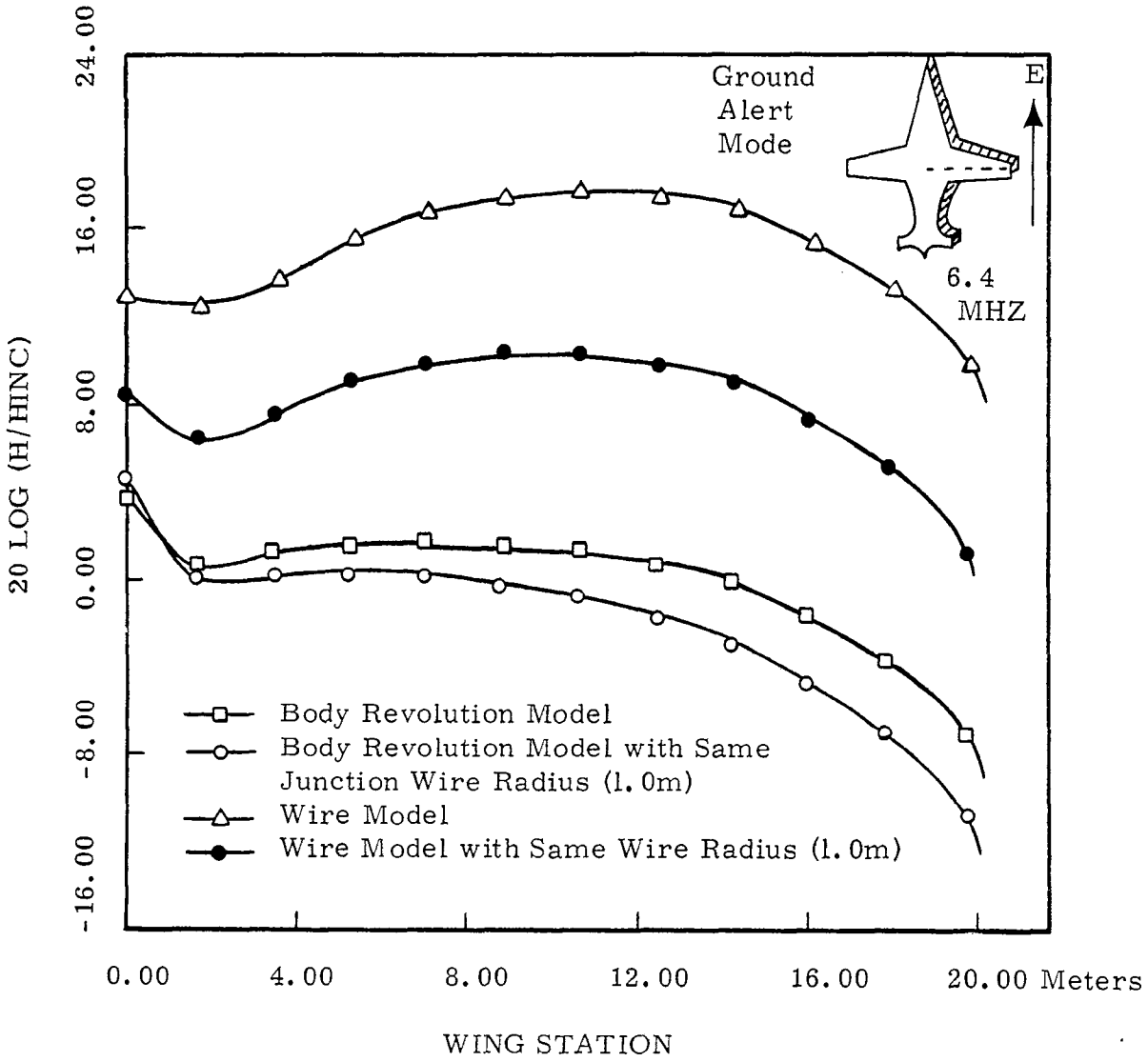

Figure 43: Wing Current Density for the B-1 in the Ground Alert Mode with Top-side Incidence, h = 4.1 Meters

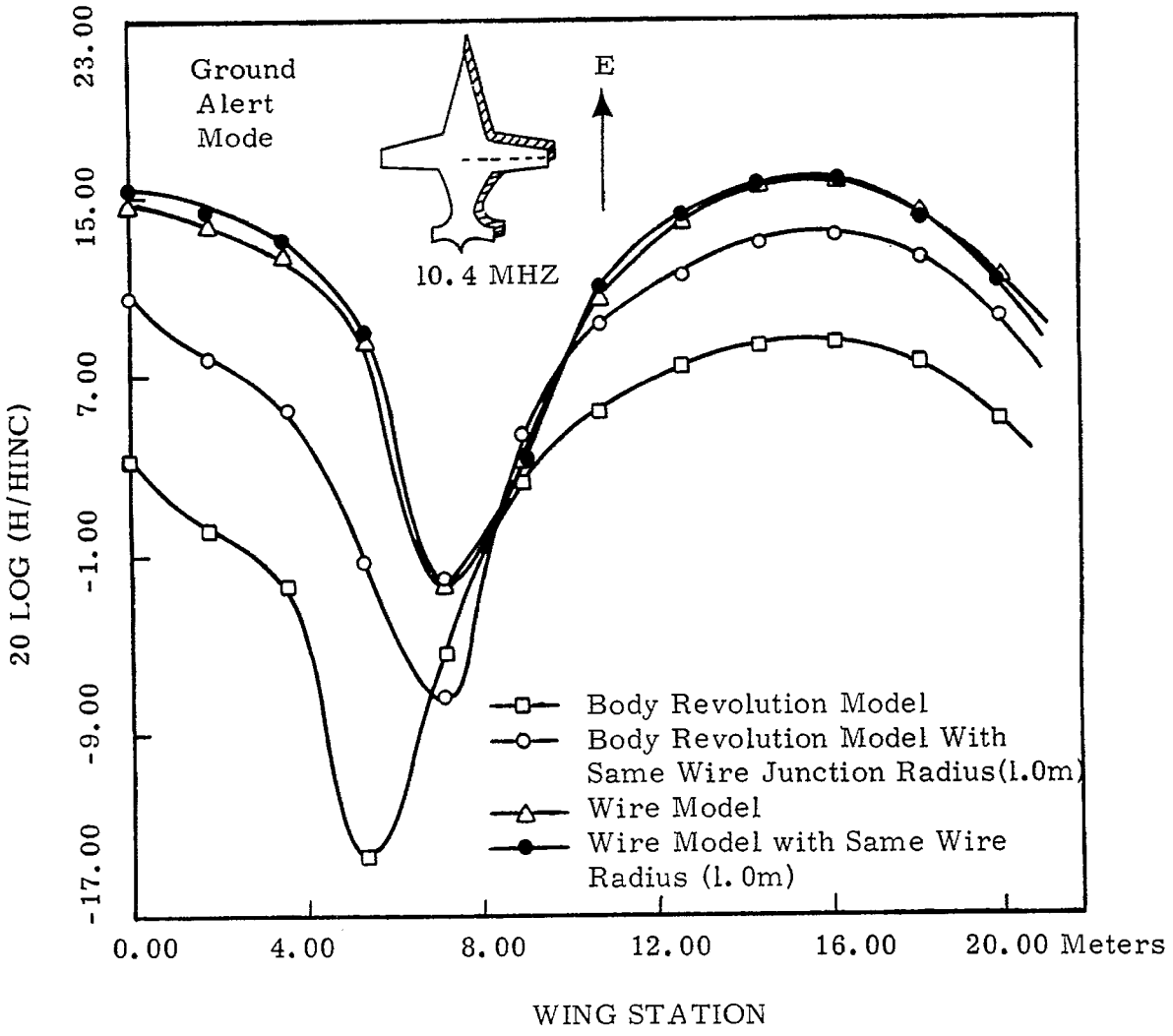

Figure 44: Wing Current Density for the B-1 in the Ground Alert Mode with Top-side Incidence, **h = 4.1 Meters**

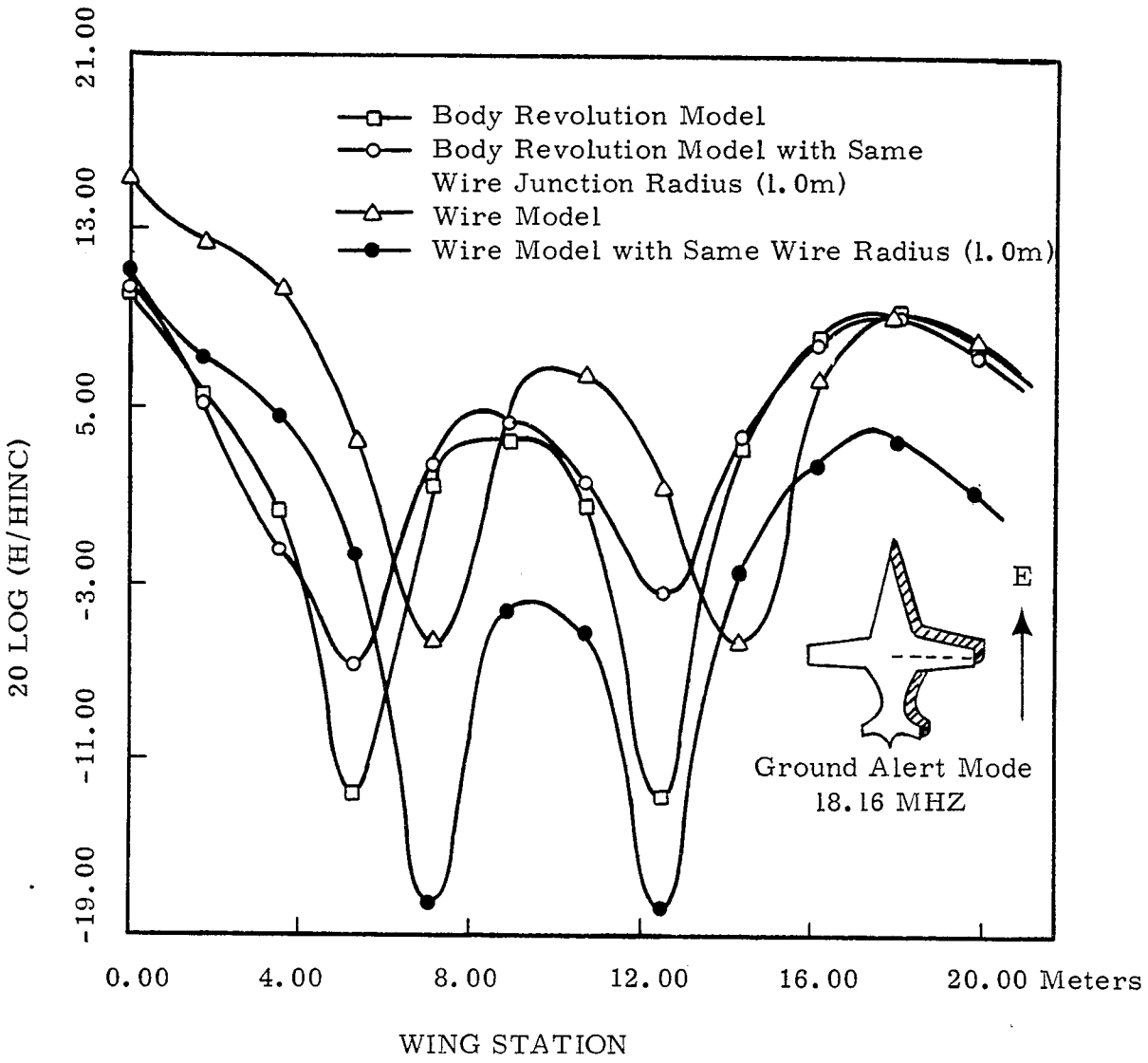

Figure 45: Wing Current Density for the B-1 in the Ground Alert Mode with Top-side Incidence, **h = 4.1 Meters**

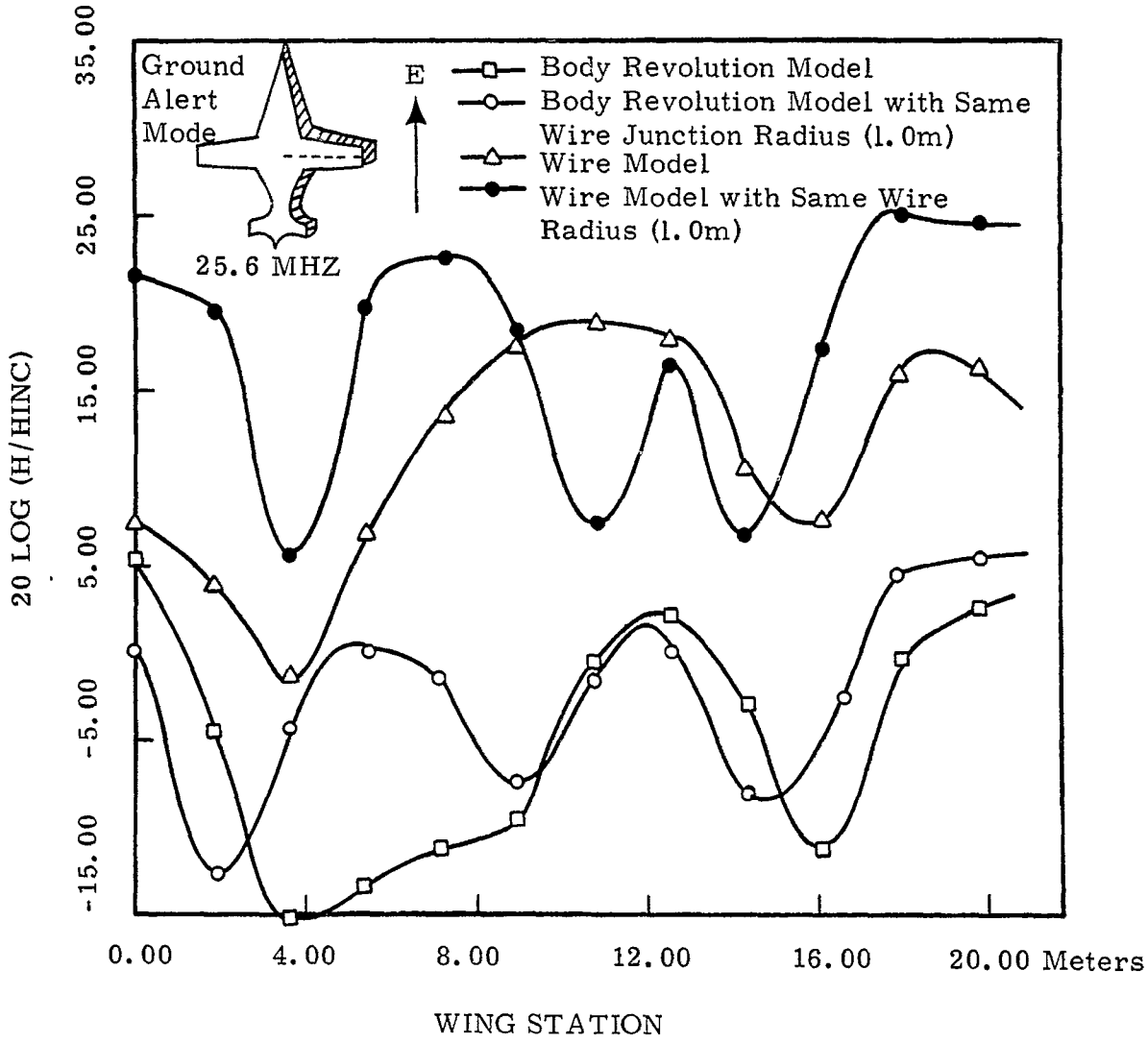

Figure 46: Wing Current Density for the B-1 in the Ground Alert Mode with Top-side Incidence, **h = 4.1 Meters**

SECTION IV

CONCLUSION

It has been shown that the body of revolution model of an aircraft is an improvement on the wire model for calculating induced current and charge on the aircraft. Comparison with measured data reveals that the body of revolution model yields aircraft current densities that agree with measurement within 6 db generally. Moreover it has been shown that the results from the body of revolution formulation compare favorably with other theoretical results.

A few data are presented from the Singularity Expansion Method calculations and for the ground alert mode configuration.

APPENDIX

AVERAGE RADIUS FOR WIRE COUPLING

Along the axis of a given wire the electric field contribution arising from the currents on other wires can be approximated to first order by using the wire filament expressions. But near the intersection of wires this approximation deteriorates. Even so, good results have been obtained by using it (ref. 8). However if the wire circumference is divided into filamentary strips and the circumferential current distribution is known then integrating the filamentary contributions would yield exact expressions for the electric field components along the wire axes. Since the circumferential current distributions are known only to be approximately uniform for electrically thin wires then a simple approximation can be obtained to account for the finite wire radius without having to evaluate the envolved integrals that would be required for the exact field expressions.

Consider the wires shown in figure A1. If the field is to be evaluated along the horizontal wire, then the current filaments constituting the current on the intersecting wire will each be at a different radial distance from points along the horizontal wire. Consider the cross section shown in figure A1. The radial distances to the point shown on the axis of the horizontal wire is

$$r = \sqrt{r_o^2 + a^2 + 2ar_o \cos\theta \sin\gamma}$$

where θ locates each infinitesimal filament around the cross section and the other parameters are shown in the figure. The average radial distance of the surface filaments is

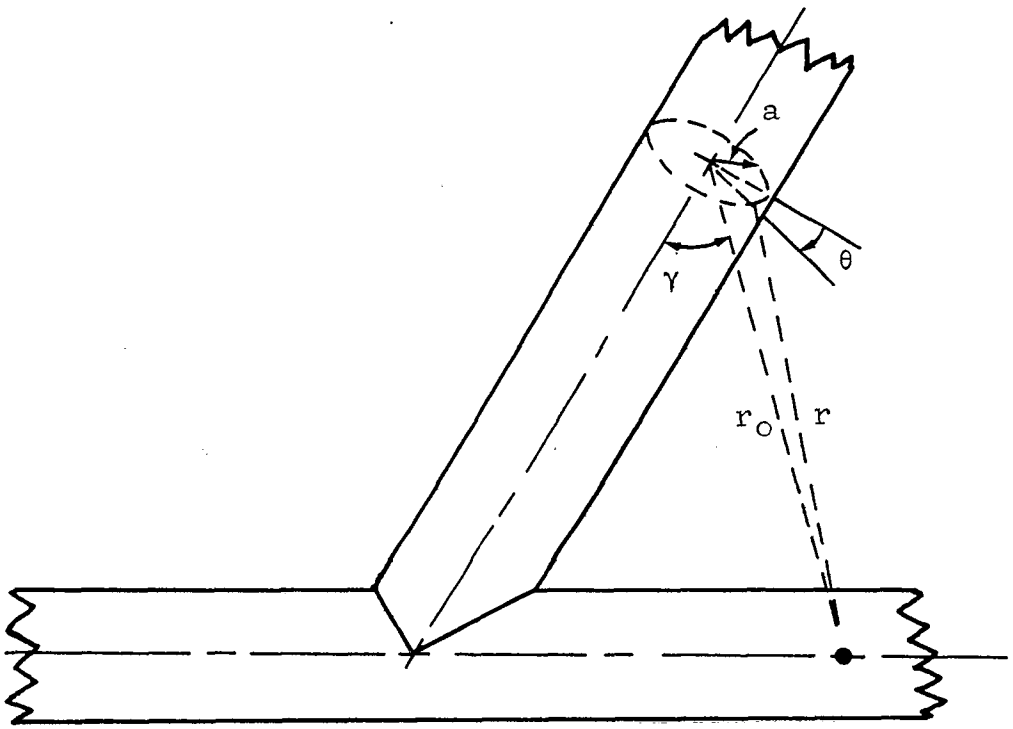

Figure A-1: Intersecting Wires with Finite Radii

$$\langle r \rangle = \frac{1}{\pi} \int_0^{\pi} \sqrt{r_o^2 + a^2 + 2ar_o \cos\theta \sin\gamma}\, d\theta$$

After some mathematical manipulation the foregoing becomes

$$\langle r \rangle = \sqrt{r_o^2 + a^2} \left\{ 1 - \frac{1}{4} \left[\frac{a/r_o}{1 + (a/r_o)^2} \right]^2 \sin^2\gamma + \cdots \right\}$$

And if

$$r_o > a/20$$

then

$$\langle r \rangle \simeq \sqrt{r_o^2 + a^2}$$

Hence the finite wire radii can be accounted for at least to a first order approximation by using the above radial distances and the simple filamentary current electric field expressions.

REFERENCES

1. Taylor, C. D. and Crow, T. T., "Induced Electric Currents on Some Configurations of Wires: Part I. Perpendicular Crossed Wires," AFWL Interaction Note 85, November 1971.

2. Crow, T. T., Shumpert, T. H. and Taylor, C. D., "Induced Electric Currents on Some Configurations of Wires: Part II. Non-perpendicular Crossed Wires," AFWL Interaction Note 100, April 1972.

3. Taylor, C. D., "On the Exact Theory of a Prolate Spheroidal Antenna," Radio Science, Vol. 2. (New Series), pp. 351-360, March 1967.

4. Shumpert, T. H., Crow, T. T., and Taylor, C. D., "Induced Electric Currents on Configurations of Thick Wires, Perpendicular Crossed Wires," AFWL Interaction Note 103, May 1972.

5. Curtis, W. L., "Current and Charge Distribution on Aircraft," Joint EMP Technical Meeting, Kirtland AFB, September 1973.

6. Taylor, C. D., "A Simple Procedure for Estimating the Current Induced on Cylinder-like Conductors Illuminated by EMP," AFWL Interaction Note 176, July 1973.

7. Taylor, C. D. and Wilton, D. R., "The Extended Boundary Condition Solution of the Dipole Antenna of Revolution," Interaction Note 113, June 1972.

8. Crow, T. T., Graves, B. D. and Taylor, C. D., "The Singularity Expansion Method as Applied to Perpendicular Crossed Cylinders in Free Space," AFWL Interaction Note 161, October 1973.

9. King, R. W. P. and Wu, T. T., "Analysis of Crossed Wires in a Plane-wave Field," AFWL Interaction Note 216, July 1974.

10. E. F. Knott, "Surface Field Measurements," AFWL Interaction Application Memo No. 5, September 1974.

11. Schelkunoff, S. A. and Friis, H. T., Antennas: Theory and Practice. John Wiley, New York, 1952.

12. Mei, K. K., "On the Integral Equations of Thin Wire Antennas," IEEE Trans. Ant. Prop., AP-13, pp. 374-378, May 1965.

13. Chao, H. H. and Strait, B. J., "Computer Programs for Radiation and Scattering by Arbitrary Configurations of Bent Wires," AFWL Interaction Note 191, September 1970.

D/21785

14. Butler, C. M., "Currents Induced on a Pair of Skew Crossed Wires," IEEE Trans. Ant. Prop., AP-20, pp. 731-736, November 1972.

15. Richmond, J. H., Schwab, L. M., and Wickliff, R. G., "Tumble-Average Radar Backscatter of Some Thin-Wire Chaff Elements," IEEE Trans. Ant. Prop., AP-22, pp. 124-126, January 1974.

16. Sayre, E.P., "Junction Discontinuities in Wire Antenna and Scattering Problems," IEEE Trans. Ant. Prop., AP-21, pp. 216-217, March 1973.

17. Miller, E.K., Bevensee, R. M., Poggio, A. J., Adams, R., Deadrick, F. J., and Lnadt, J. A., "An Evaluation of Computer Programs Using Integral Equations for the Electromagnetic Analysis of Thin Wire Structures," AFWL Interaction Notes, Note 177, March 1974.

18. Mittra, R. and Ko, W. L., "A Finite Difference Approach to the Wire Junction Problem," to be submitted for publication.

19. King, R. W. P. and Burton, R., private communication.

20. Richmond, J. H., "Radiation and Scattering by Thin-Wire Structures in a Homogeneous Conducting Medium," IEEE Trans. Ant. Prop. (Computer Program Descriptions), Vol. AP-22, pp. 365, March 1974.

☆U.S. GOVERNMENT PRINTING OFFICE: 1975—A-0298/(42) 20